Process Biochemistry 129 (2023) 170–184

Contents lists available at ScienceDirect

Process Biochemistry

journal homepage: www.elsevier.com/locate/procbio

Physicochemical properties of green synthesised ZnO nanoparticles and utilisation for treatment of breast cancer

Raunak Saha [a,1], Karthik Subramani [b,1], Sreenath Dey [c], Saheri Sikdar [d], Aran Incharoensakdi [b,e,*]

[a] Centre for Nanoscience and Technology, K S Rangasamy College of Technology, Tiruchengode, Tamil Nadu, India
[b] Laboratory of Cyanobacterial Biotechnology, Department of Biochemistry, Faculty of Science, Chulalongkorn University, Bangkok 10330, Thailand
[c] Department of Biotechnology, Indian Institute of Technology Hyderabad, Telangana 502285, India
[d] Department of Biochemistry and Molecular Biology, Universität Bremen, Bibliothekstraße 1, 28359 Bremen, Germany
[e] Academy of Science, Royal Society of Thailand, Bangkok 10300, Thailand

ARTICLE INFO

Keywords:
Green synthesis
ZnO nanoparticles
Apoptotic pathway
MCF-7
Cancer treatment

ABSTRACT

Metal oxide nanoparticles with unique properties have recently attracted much attention as a potential smart material for treatment of cancer. The inherent structural and ionic defects in ZnO nanoparticles allow the formation of intracellular superoxide and hydroxyl radicals after entering a cancer cell causing damage on DNA and preventing subsequent replication. However, the full extent of the DNA damage and the knock-on effect with respect to protein synthesis is not copiously comprehended. This study tries to tune the cytotoxic activity of ZnO nanoparticles in virtue of physicochemical property against human breast cancer cell (MCF-7) via reactive oxygen species (ROS) induced DNA damage leading to apoptosis. In order to produce an array of different size and shape of ZnO nanoparticles with varying structural defects, this study utilised the unique phytochemicals of *Terminalia arjuna, Swertia chirayita,* and *Psidium guajava* as the active reducing agents for the formation of the nanoparticle from the mineral salt. Variations in the created nanoparticle size and relative structural defects have caused a consequential surge in ROS production inside cancer cells resulting in enhanced effectiveness of ZnO nanoparticles for cancer treatment.

1. Introduction

Cancer is a group of heterogeneous and complex disease involving abnormal cell growth, i.e., some of the cells start dividing uncontrollably without stopping leading to tumour formation [1–4]. Observational studies have hinted that there are various reasons for cancer cell development in the human body such as DNA damage due to chemo genes, oncogenes and oncoviruses [5–7]. Out of all the major cancers, breast cancer has been one of the most diagnosed cancers in females, i.e., accounting for almost one in four cancer cases [8]. Breast cancer refers to formation of cancerous cell originating from the lining of milk duct, the condition is characteristic to development of lumps in breast and change of breast size [9–11]. For the last few decades cancer continues to be a worldwide killer, despite the number of researchers developing new drugs and materials to combat cancers [12]. Several conventional approaches like chemotherapy [13–15], radiotherapy [16–18], and even immunotherapy [19–21] are adopted to protect patients against cancer, but the outcomes shown by these studies are negligible. Therefore, the researchers are trying to shift their focus from conventional medicinal approaches to the use of nanostructured materials for exploiting their atom-like behaviour in anticancer treatment [22].

Nanomaterials or particles in a size ranging between 1 and 100 nm, owing to their unique interactions with biological systems, have extensive use in tumour imaging in vivo [23,24], biomolecular imaging [25,26], marker development for cancer [27,28] and smart delivery systems [29,30]. New therapeutic approaches are developing rapidly with the focus on the development of anticancer drugs based on exploiting the cytotoxic properties of nanoparticles [31]. Over the last few years, various bio-engineered metal/metal oxide nanoparticles such as Ag, NiO, TiO_2 have been reported to show anticancer effect on cancer

* Corresponding author at: Laboratory of Cyanobacterial Biotechnology, Department of Biochemistry, Faculty of Science, Chulalongkorn University, Bangkok 10330, Thailand.
E-mail addresses: aran.i@chula.ac.th, in.aran@gmail.com (A. Incharoensakdi).
[1] These authors have contributed equally to this work and share first authorship.

https://doi.org/10.1016/j.procbio.2023.03.016
Received 26 December 2022; Received in revised form 30 January 2023; Accepted 14 March 2023
Available online 16 March 2023

cells [32–34]. For our study, however, we focused on ZnO nanoparticles: owing to their structural instability, as well as their ability to form superoxide and hydroxyl radical inside the cell that can cause DNA damage [35,36]. Moreover, ZnO based nanoparticles have been reported to be extremely versatile materials as their physicochemical properties can be easily controlled [37,38]. It is important to exploit these certain traits of ZnO nanoparticles for an effective anticancer activity against MCF-7 breast cancer cells in virtue of changes in nanoparticles physicochemical properties.

ZnO nanoparticles produced by traditional methods show high purity but the reaction by-products are toxic and difficult to remove [39–41]. To reduce the toxic nature and to ease up the synthesis process, researchers are trying to shift their focus to green chemistry, i.e., designing synthesis routes that minimise the use or production of hazardous materials by employing natural reducing agents such as phytochemicals for the preparation of nanomaterials [42–46]. In this study, three plants were mainly selected for ZnO nanoparticles green synthesis, i.e., *Terminalia arjuna* (*T. arjuna*), *Swertia chirayita* (*S. chirayita*), and *Psidium guajava* (*P. guajava*). These plants have been shown to contain phytochemicals that helps in stabilisation and coordination of Zn (II) during nanoparticle formation. Previous studies on these plants regarding the biosynthesis of ZnO nanoparticles with respect to various processing parameters showed that the produced nanoparticles had dissimilar physico chemical traits due to the variation in the plant phytochemicals [47–49]. In view of this characteristic trait, *T. arjuna, S. chirayita* and *P. guajava* are ideal plants for ZnO nanoparticles synthesis through sustainable green chemistry.

In this study, zinc precursor was reduced to zinc oxide nanoparticles using different phytochemicals from *T. arjuna, S. chirayita* and *P. guajava* through a hydrothermal route of synthesis. A hydrothermal route of synthesis is a synthesis route employing a constant temperature and pressure using a Teflon line autoclave which greatly controls and stabilises the reaction kinetics. Hence, it is the most suitable synthesis route to form nanoparticles with controlled uniform size distribution and favourable physicochemical property. [47–49]. The three ZnO nanoparticles were thoroughly assessed for their physicochemical and cytotoxic properties. Furthermore, to highlight a potential of the nanomaterial in biomedical application, cytotoxic activity against the zebra fish (*Danio rerio)* was also assessed. In addition, the study also evaluated a comparative assessment of ZnO nanoparticles based on anticancer efficacy against MCF-7 cells. The study not only showcases a relative assessment of nanoparticles but also opens up new boundaries on exploiting the effectiveness of ZnO nanoparticles for anticancer activity owing to changes in physicochemical properties.

2. Materials and methods

2.1. Materials

2.1.1. Preparation of crude phytochemical extract

For the preparation, freshly acquired *T. arjuna* bark, *S. chirayita* stem and *P. guajava* leaves were collected from West-Bengal, India. The harvested phyto-specimens were dried (14 days, at room temperature, away from direct sunlight) before being submerged in double deionised (DD) water to remove any surface dust. The sample (10 g) was then heated at 80 ºC to reflux (2 h) in DD water (100 mL). After cooling, the aqueous solution (Optical density at 200 nm was found to be 3.97, 2.43 & 1.747 a.u. for *T. arjuna* bark, *S. chirayita* stem and *P. guajava* leaves respectively (Fig. S2)) was filtered and used immediately [48].

2.2. Synthesis of ZnO nanoparticles

Hydrothermal route was exercised during ZnO nanoparticles synthesis. Firstly, zinc acetate (18.3 g) (Merck, India) was directly added to 100 mL of prepared plant extracts (*T. arjuna, S. chirayita*, and *P. guajava*). The solutions were shifted to hydrothermal autoclave containing Teflon inner lining. The reaction parameter was maintained at 220 °C under constant pressure for 12 h and then left undisturbed in ambient temperature to cool. The solutions were then centrifuged (at 5590 g for 30 min) and washed repeatedly with DD water (4 times) to remove any by-products, followed by drying (12 h at 120 °C). It was then calcined (500 °C for 2 h) to impart a slight crystallisation in the ZnO particles [49]. The obtained calcined ZnO nanoparticles were marked ZnO^{Ta}, ZnO^{Sc}, and ZnO^{Pg} corresponding to the three plant extracts (*T. arjuna, S. chirayita*, and *P. guajava*).

2.3. Characterisation of ZnO nanoparticles

To draw a correlation between the synthesised nanoparticles structural properties with respect to their phytochemicals, synthesised nanoparticles (ZnO^{Ta}, ZnO^{Sc}, and ZnO^{Pg}) were examined using X-ray diffractometer (X′ Pert Pro, PANalytical, Almelo, The Netherlands). The diffraction spectra were recorded in a 2θ range from 10° to 80° at 293 K at step scan mode of 0.02°. Functional groups in the prepared analytes were assessed using an ATR-FTIR spectrometer (Nicolet IS50, Thermo-Fisher Scientific, USA) in a frequency region between 4000 cm^{-1} to 400 cm^{-1} [47].

The average particle size distribution of synthesised ZnO nanoparticles was recorded using a Photon correlation spectroscopy (Nanophox, Sympatec, Clausthal-Zellerfeld, Germany). Surface area measurements were evaluated by a three-point BET plot (BET Autosorb AS-1MP; Quantachrome, Boynton Beach, FL) using nitrogen adsorption-desorption measurements over the prepared ZnO nanoparticles [39]. For morphological and elemental analysis, ZnO nanoparticles were subjected to scanning electron microscope coupled with an energy dispersive X-ray spectrometer (SEM-EDX, JSM 6360 JEOL, Japan) [48].

The excitation and emission spectra of the samples were procured using UV–visible spectrophotometer (UV-Vis, Cary 8454; Agilent Technologies, Singapore) and photoluminescence (PL) spectroscope (Cary Eclipse; Agilent Technologies, Singapore). To perform this comparative optical assessment in virtue of phytochemicals, the ZnO nanoparticles diluents (25 μg mL^{-1}) were monitored and compared with respect to excitation and emission spectra [49].

Surface chemical composition and defect analysis were assessed using X-ray photoelectron spectroscope (XPS; JEM-2100 F) with an Al Kα having a binding energy of 1486.6 eV. For the surface charge analysis, Zeta potential analyser (Malvern Instruments Ltd., GB) was used.

2.4. Antioxidant activity

2,2-diphenylpicrylhydrazyl (DPPH) free radical scavenging assessment was employed to determine the ZnO nanoparticles (ZnO^{Ta}, ZnO^{Sc}, and ZnO^{Pg}) antioxidant activity. One mL of methanol (50%) along with various concentrations (5, 10, 15, and 20 mg mL^{-1}) of analytes (ZnO^{Ta}, ZnO^{Sc}, and ZnO^{Pg}) were added to 1 mL of 1 mM DPPH (Sigma-Aldrich; U.S.A.) and incubated at 37 °C under dark conditions for 30 min. Ascorbic acid was used as the control. Following the exposure of the analytes to the DPPH solution, the absorbance at 517 nm was measured and the antioxidant activity was estimated using the following equation,

$$\text{DPPH Scavenging (\%)} = \frac{CA-TA}{CA} \times 100.$$

where CA and TA are control absorbance and test absorbance respectively (Vitamin-C was used as the positive control) [50].

2.5. In-vivo toxicity evaluation

To assess the acute toxicity of the prepared nanoparticles, the mortality of the zebra fish (*Danio rerio)* was recorded after exposure to the prepared ZnO samples (ZnO^{Ta}, ZnO^{Sc} and ZnO^{Pg}) for 72 h. *Danio rerio (D. rerio)* embryo was used as the test model for this study due to its high transparency, and also because of its similar genomic resemblance to the human genome. The assessment was conducted on 25 selected zebra fish

embryos treated with 25, 50, 75, 100 and 200 μg mL^{-1} ZnO samples according to OECD-203 guidelines [51].

2.6. Maintenance of cell culture and exposure to nanoparticles

MCF-7 cells were procured from National Centre for Cell Sciences (NCCS), Pune, India. The cells were maintained using Dulbecco's modified eagles' medium (DMEM) supplemented by foetal bovine serum (FBS), penicillin and streptomycin cocktail (ThermoFisher Scientific, USA). The obtained cancer cells were maintained under 5% humidified CO_2 atmosphere at 37 °C. The medium was changed every 2 days and subcultured once every week.

For the in-vitro assessments, the MCF-7 cells were seeded at 10^5 cells per well in a 24 well plate and incubated for 24 h at 37 °C before the addition of ZnO NPs suspension. The sonicated stock solutions of ZnO nanoparticles prepared at different concentrations (0, 5, 10, and 20 μg mL^{-1}) in cell medium were added to the plates and incubated for various times [52].

2.7. Measurement of intracellular reactive oxygen species (ROS)

2,7-dichlorofluorescein diacetate dye or (DCFDA) assay (ThermoFisher Scientific; USA) was used for determining the intracellular ROS. For this assessment of cells following 6 h of ZnO nanoparticle exposure, the cells were incubated with DCFDA dye for 30 min at 37 °C. Fluorescence intensity was measured spectrophotometrically using a microplate reader at 528 nm [52].

2.8. Cytotoxicity assay

2.8.1. MTT assay

For cell viability assessment using 3-[4,5-imethylthiazol-2-yl]− 2,5 diphenyl tetrazolium bromide (MTT) assay (ThermoFisher Scientific; USA), the 24 h ZnO nanoparticles exposed cells were treated with MTT (5 mg mL^{-1}) and incubated for 4 h at 37 °C. Dimethyl sulfoxide was then added which dissolved MTT derivative to give purple formazan, which was measured using a microplate reader at 570 nm and the percentage of cell death was determined using the equation,

$$D(\%) = \frac{A_0 - A_e}{A_0} \times 100$$

where D% represents the percentage cell death and A_0 and Ae are absorbance of control and experiment, respectively [53].

2.8.2. Neutral red uptake (NRU)

For cell viability assessment using NRU assay (ThermoFisher Scientific; USA), the 24 h ZnO nanoparticles exposed MCF-7 cells were incubated with neutral red solution at 37 °C for 3 h. Cell viability assessed by neutral red uptake by MCF-7 cells was monitored by measuring the absorbance at 540 nm [54].

2.8.3. Lactate dehydrogenase (LDH) release assay

LDH release upon ZnO analyte exposure was determined using commercial LDH Kit (Thermoscific; USA). For the assessment, the MCF-7 cells treated with ZnO for 24 h were washed with PBS followed by addition of LDH reagent and incubated for 15 min at 37 °C before measuring the absorbance at 490 nm. The LDH activity in the cell medium can be directly attributed to non-viable cells present [55].

At least 5 independent repeats were performed for every cytotoxic test to showcase the reproducibility of the effect of nanoparticle on biochemical activity.

2.9. Genotoxic assay (comet assay)

To evaluate DNA damage of ZnO exposed MCF-7 cells, comet assay was used. MCF-7 cells exposed to ZnO nanoparticles for 24 h were coated onto a comet slides pre-coated with normal melting agarose followed by the loading of the suspended cells (100 μL) mixed with 100 μL of 1% low melting agarose. Slides were then maintained at 4 °C for 12 h followed by exposing to chilled lysis solution (Bio-techne; India). Fluorescence microscope was used to assess the DNA damage in each cell [56]. The whole assessment was repeated thrice.

2.10. Assessment of cytochrome c release

Cytochrome c release assay of ZnO nanoparticle exposed MCF-7 was performed to confirm apoptotic pathway using Cyt-c ELISA Kit (LS Bio, Seattle) according to manufacturer's protocol [57].

2.11. Apoptosis

2.11.1. Western blot analysis

The nanoparticle showing the most promising result towards the biochemical assay (ThermoFisher Scientific; USA) was pelleted and lysed using (radioimmuno precipitation) lysis buffer and protease inhibitor cocktail [58]. Bovine serum albumin was used as the standard. After resolving the proteins (40 μg per lane) by SDS-polyacrylamide gel electrophoresis, the protein samples were transferred to a nitrocellulose membrane and probed with anti-human primary antibodies (1:1000) against β-actin, JNK, phosphor-JNK, ERK (1/2), phosphor-ERK (1/2), p38, phosphor-p38, caspase-9, p53, phosphor-p53, Bcl2, Bax, and nuclear factor kappa-β (NF-Kβ) for 1 h at room temperature (Thermofisher Scientific, USA). The reaction was blocked by 5% non-fat milk for 1.5 h at room temperature. This was followed by the incubation for 1.5 h at room temperature using secondary anti-primary antibody conjugated to horse radish peroxidase [58]. The protein bands were visualised for the assessment of the apoptotic pathway adopted by the MCF-7 cell line after ZnO exposure.

2.12. Morphological study

MCF-7 cells exposed to different concentrations of ZnO nanoparticles (0, 5, 10, and 20 μg mL^{-1}) were viewed under a standard microscope (20X magnification) with a CCD image sensor.

3. Results and discussion

3.1. Physicochemical properties

Physicochemical properties and biological activity of the prepared ZnO^{Ta}, ZnO^{Sc} and ZnO^{Pg} nanoparticles such as crystalline nature, purity, toxicological and anticancer activity were comprehensively analysed in details. Fig. 1a shows the XRD patterns of calcined ZnO nanoparticles. Miller indices of each Braggs peaks shown in the XRD spectra confirm the polycrystalline nature of the synthesised ZnO nanoparticles [59].

The XRD patterns of ZnO^{Ta}, ZnO^{Sc} and ZnO^{Pg} samples showed diffraction angle peaks at 2θ (Degree) = 31.68, 34.37, 36.19, 47.54, 56.7, 62.93 and 67.85 corresponding to the diffraction planes of (100), (002), (101), (102), (110), (103) and (112) respectively [48]. As seen from the XRD spectra (Fig. 1a), crystalline structure of the analytes can be suggested as wurtzite structure (hcp structure) and also contrasts to the JCPDS file no. 79–0208 [60]. Moreover, absence of any other diffraction peaks suggests that the prepared ZnO nanoparticles is free of any other impurities [61]. Furthermore, from the XRD spectra we can see a decrease in peak intensity in the order of ZnO^{Ta}, ZnO^{Sc} and ZnO^{Pg}, inferring that the ZnO nanoparticles synthesised from the extracts of *T. arjuna*, show higher crystallinity compared to the ZnO nanoparticles synthesised using the nanoparticles prepared using the other phytoconstituents.

Scherrer formula was used to ascertain the ZnO nanoparticles average crystal size from XRD spectra and was seen to change from one

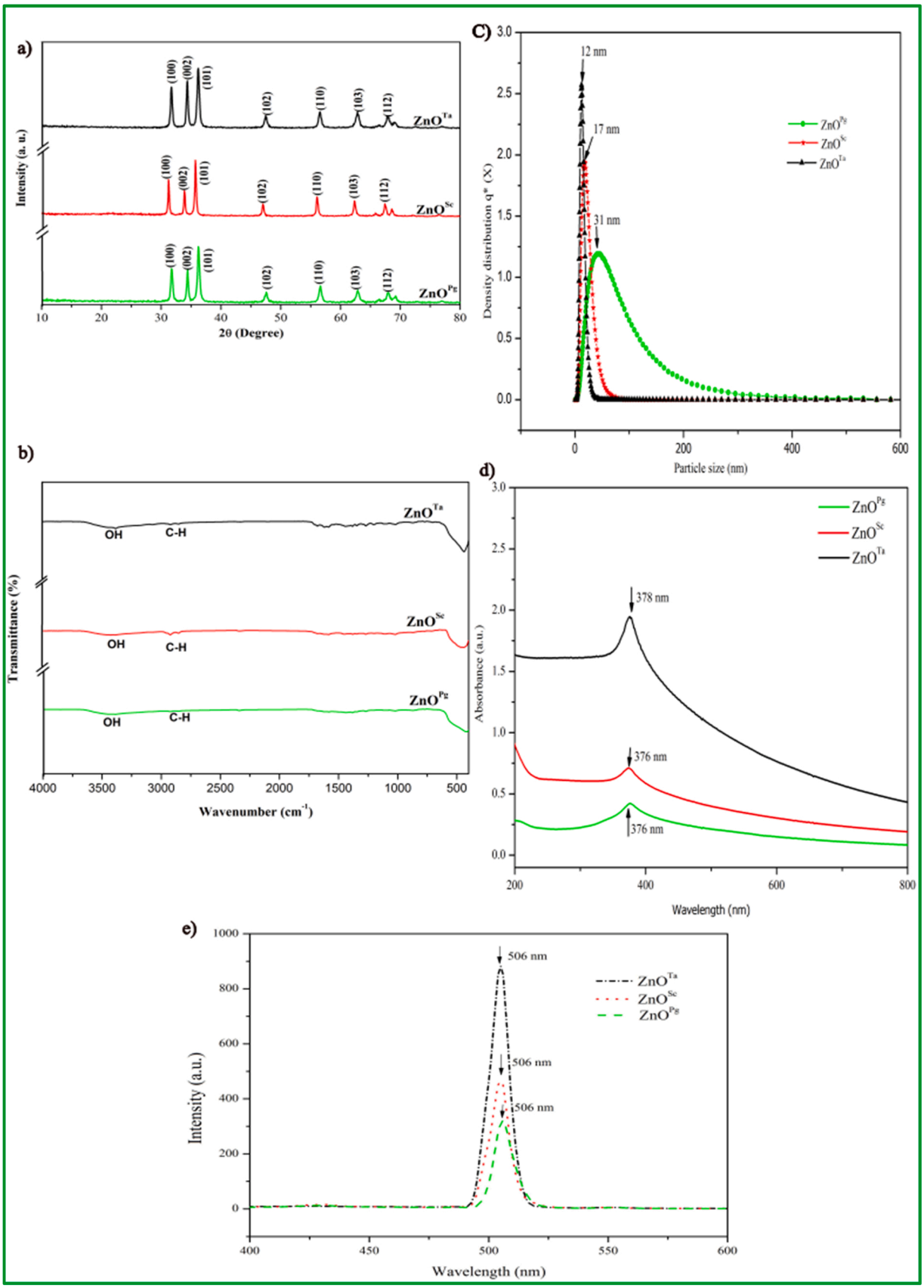

Fig. 1. Physicochemical properties of the prepared ZnO nanoparticles: a) X-Ray Diffraction spectra, b) Fourier Transform Infra-red spectra, c) Particle size distribution, d) UV-Absorbance and e) Photoluminescence spectra.

phytochemical to another [47,49]. For comparative assessment, ZnO^{Ta} showed extremely small size (12.83 nm) compared to its counterparts (ZnO^{Sc} and ZnO^{Pg}; 17.40 and 33.26 nm respectively) which suggested that phytoconstituents of *T. arjuna* were more effective in stabilising and controlling the growth rate (Table S1).

Fig. 1b depicts the FTIR spectra of the prepared nanoparticles. The figure clearly depicts that the procured IR spectrums of all the ZnO nanoparticles synthesised (ZnO^{Ta}, ZnO^{Sc} and ZnO^{Pg}) are similar. Strong absorption peaks below 400 cm^{-1}, confirms ZnO presence [62]. Transmittance peaks at 3500, 2830, and 3000 cm^{-1} might be due to the presence of O-H stretching mode and stretching mode vibration of alkane groups respectively. Therefore, looking at the FTIR spectra, one can conclude that the nanoparticles synthesised using the phytoconstituents of *T. arjuna, S. chirayita*, and *P. guajava* plant extract show similar results and differences in the phytochemicals used have no effect on the FTIR spectra. Furthermore, we can suggest that the observed impurities seen in the FTIR spectra of the prepared analytes, might be due to the higher surface absorption of ambient water or the impurities might have originated from plant phytoconstituents (Fig. S1) used as the reducing agent [49].

ZnO nanoparticles prepared using plant extract of *T. arjuna* as the reducing agent for the zinc precursor show lowest average particle size (Fig. 1c). The particle size distribution was also evaluated showing the average particle size distribution to be in nm range. The results indicate that all the phytochemicals in *T. arjuna, S. chirayita, and P. guajava* plant extract are effective in reducing Zn acetate to ZnO in nano range. It is noted that there is a tangential increase in the particle size in the order of ZnO^{Ta}, ZnO^{Sc} and ZnO^{Pg}. Moreover, differences in the phytochemicals can result in the change in the particle size formed. From our previous comparative studies on the use of plant phytochemicals for the biosynthesis of ZnO nanoparticles using various processing parameter such as sonication, wet-chemical and hydrothermal, we found that hydrothermal green synthesis showed lower size distribution. This is due to the fact that during hydrothermal synthesis the reaction temperature increases slowly from the start at room temperature till 200 °C. During the initial phase of reaction, the reaction kinetics is stabilised by the plant phytochemicals. However, following a threshold phytochemical decomposition the temperature of the reaction slowly increases by thermal decomposition of the mineral salt after which the mineral salt is thermally degraded. This is followed by the stabilisation of the particle formation to nano regime by high temperature pressure [47,48].

However, in our study we did not observe any acetate peaks in the FTIR suggesting that most of the zinc salts were decomposed. Moreover, all plants have their own characteristic phytochemicals and concentration, leading to variation in reaction kinetics [49]. We suggest from the aforementioned result that the *T. arjuna* plant extract was more efficient in stabilising the reaction leading to a lower particle size distribution.

Table S2 and Fig. S3 show that surface area of ZnO nanoparticles prepared using plant extract of *T. arjuna* extract as the reducing agent for the zinc precursor was higher (253.7 m^2g^{-1}) than that prepared using *S. chirayita* and *P. guajava* (228.1, and 217.7 m^2g^{-1} respectively) plant extracts. This reveals that particle size can influence and tune surface area, which in turn can be tuned by phytochemicals.

The UV absorption spectra of the ZnO nanoparticles i.e., ZnO^{Ta}, ZnO^{Sc} and ZnO^{Pg}, show UV absorption at wavelength of 378, 376 and 376 nm respectively (Fig. 1d). Planck's equation ($E = h/C\ \lambda\ h$, C, and λ are Planck's constant, speed of light and excitonic wavelength respectively) was used to calculate the energy band-gap of the prepared ZnO^{Ta}, ZnO^{Sc} and ZnO^{Pg} nanoparticles [47,63]. Interestingly, the absorption wavelength of the prepared ZnO nanoparticles remains unchanged, and the band-gap of the ZnO nanoparticles was found to be 3.3 eV which is in line with the previous study [64]. It is noted that the prepared nanoparticles show little change in the excitonic wavelength, whereas there is a considerable change in absorption intensity of the UV-Vis spectra. Compared to ZnO^{Sc} and ZnO^{Pg} nanoparticles, ZnO^{Ta} nanoparticles show higher maximum absorption intensity which might be related to the entrapment of emission occurring during the UV irradiation of the suspended nanoparticles [65]. Interestingly, this aforementioned phenomenon results in a shift in electron density, i.e., Zn^{+} absorbs photonic energy leading to increased photonic absorption as reported in earlier studies [48,49]. This observation helps in the inference that the ZnO nanoparticles prepared using the *T. arjuna arjuna* plant extract as the reducing agent show smaller particle size than that using other nano samples, i.e., ZnO^{Sc}, and ZnO^{Pg} as confirmed by prior assessment. The study correlates the tweaking nature of the ZnO nanoparticles by change in reaction parameter.

Fig. 1e shows the PL spectra of the prepared ZnO nanoparticles. All the analytes when excited at a wavelength of 325 nm, gave a sharp and strong green emission peak at 505 nm, which is in line with previously reported studies [14]. We can also conclude from the observation of the PL spectra that the prepared ZnO samples emission wavelengths do not alter with the change in the prepared ZnO particle size and phytochemicals used. Interestingly, the luminescence intensity decreases in the order of ZnO^{Ta}, ZnO^{Sc} and ZnO^{Pg}. Along with the aforementioned observation, the PL spectra furthermore promulgates the finding of the XRD and EDX assessment of the ZnO nanoparticles. The sample produced is extremely pure, because of the absence of any other peaks and the presence of only one major emission peak, which might be a result of structural defect [65].

According to previous reports, the green emission shown by the prepared ZnO^{Ta}, ZnO^{Sc} and ZnO^{Pg} nanoparticles is due to the singly ionised oxygen which can be more precisely attributed to the result of recombination of a photo regenerated hole with singly ionised charged state of the structural defect [48]. Moreover, the change in luminescence intensity is directly proportion to the singly ionised oxygen vacancy which in turn reflects the degree of structural/ionic defects present in the sample and is in line with previously reported studies on ZnO nanoparticles [65,66]. Therefore, the ZnO sample prepared by *T. arjuna* showing higher luminescence intensity infers that it has higher structural defects than that of the other two samples (ZnO^{Sc} and ZnO^{Pg}). The above observation is sufficient to prove that as the particle size decreases, particle crystalline defect increases.

The SEM image of the prepared ZnO^{Ta}, ZnO^{Sc} and ZnO^{Pg} are shown in Fig. 2. All the prepared ZnO nanoparticles produced through the hydrothermal method using the various plant sources show a near spherical aggregated morphology as observed in previous studies [47–49]. The distinct spherical morphology seen in all the prepared ZnO nanoparticles might be due to the effective conversion of Zn acetate to ZnO nanoparticles due to the employment of controlled high temperature and pressure during their synthesis through hydrothermal route. Moreover, prior studies have shown that the phytoconstituents of various plant species can control and stabilise the size, structure and morphology of the nanoparticles growth resulting in a variation of ZnO nanoparticle physicochemical property [67,68]. The EDX analysis confirms that the prepared ZnO nanoparticle samples are extremely pure as seen in the EDX spectra showing only the presence of Zn and O (Fig. 2). Therefore, the impurities seen in the FTIR spectra of the prepared ZnO nanoparticles might be due to the absorption of ambient water vapour.

To evaluate the surface reactivity of the prepared nanoparticles, a XPS spectrum analysis was performed and the ZnO binding energy is shown in Fig. 3. ZnO binding energy was specifically analysed to see the reactivity of the material with regards to ionic potential. From the figure, it can be clearly seen that there is a high metal oxide peak superimposed over OH peak due to a clear resemblance of a secondary peak at 531.6–531.8 eV range. Interestingly, it can be seen that the intensity of the second peak decreases in the order of ZnO^{Ta}, ZnO^{Sc} and ZnO^{Pg} inferring the presence of hydroxyl group ~~of~~ on its surface. However, the nanoparticles FTIR spectra is devoid of such high hydroxyl peak suggesting that this hydroxyl group is due to the high binding energy of the nanoparticles with the ambient water vapour [69].

To convince that there might be a high ionisation surface energy of the nanoparticles due to ionic/surface structural defect, we tried to

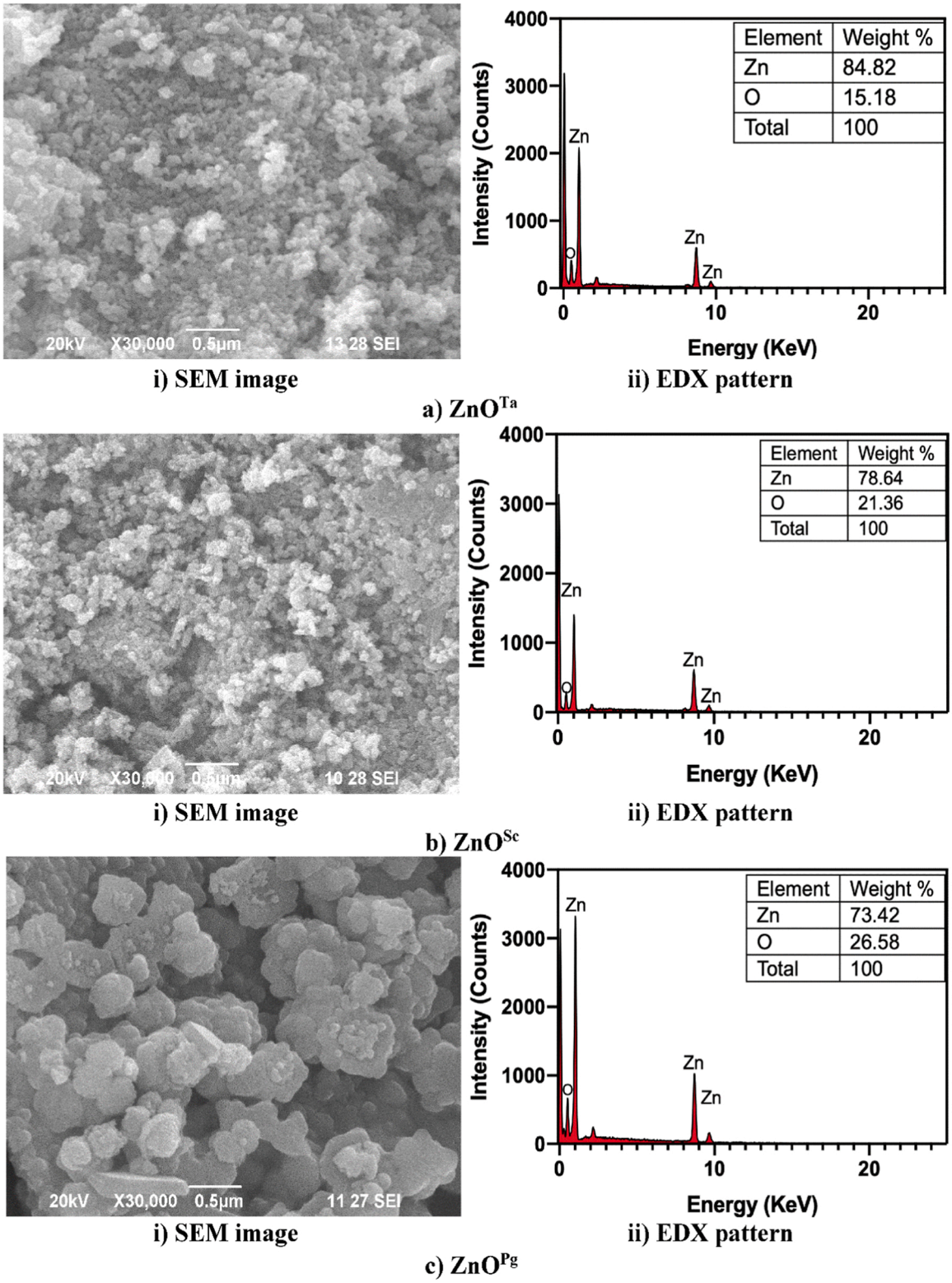

Fig. 2. Scanning electron microscope-energy dispersive X-ray analysis of the prepared ZnO nanoparticles analytes.

analyse the surface potential or Zeta potential of the nanoparticles. Table S2 shows that the surface potential shifts from − 69.8 to − 59.5 in the order ZnO^{Ta}, ZnO^{Sc} and ZnO^{Pg}. Generally, most metal oxide should be neutral. However, such neutral nanoparticles devoid of any electron and hole is rather unlikely [70]. Moreover, the high negative surface charge is characteristic of higher surface electrons which might be generated from ionic defects or structural defects during its synthesis [71].

3.2. Antioxidant activity

Fig. 4 shows the antioxidant activity of the prepared ZnO nanoparticles at various concentrations (5, 10, 15, and 20 mg mL^{-1}) assessed against di(phenyl)-(2,4,6-trinitrophenyl) iminoazarium (DPPH). The

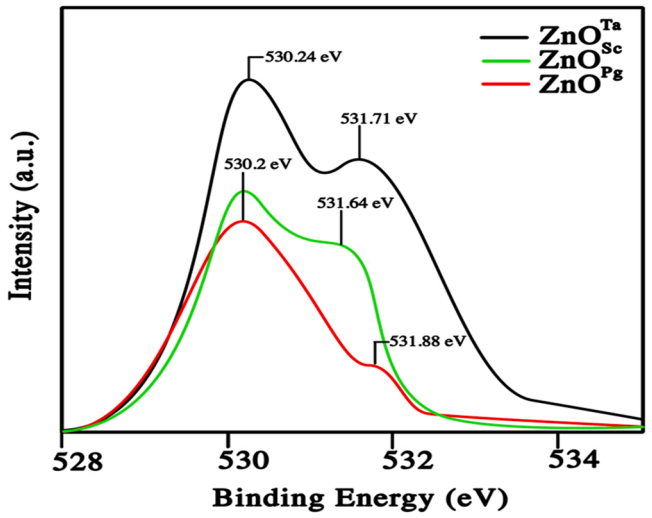

Fig. 3. XPS spectra of the prepared ZnO nanoparticles.

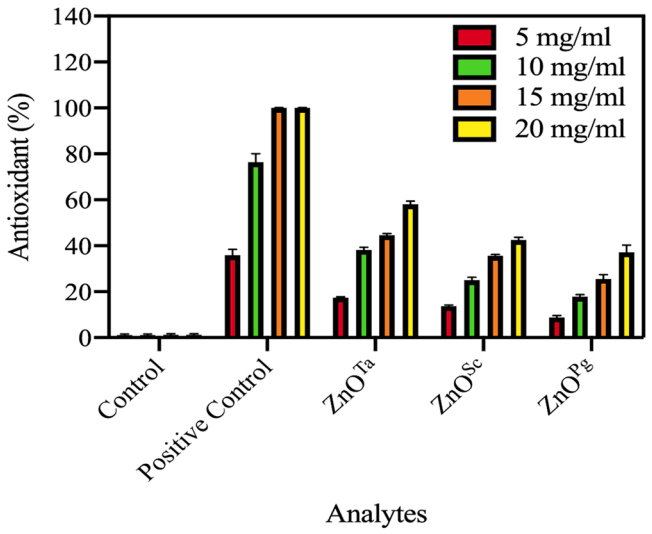

Fig. 4. Comparative antioxidant activity of the prepared ZnO nanoparticles.

prepared green synthesised ZnO nanoparticles from the plant extracts of *T. arjuna, S. chira*yita, and *P. guajava* show free radical scavenging activities against the DPPH. Moreover, the antioxidant performance of the ZnO nanoparticles prepared using *T. arjuna* was higher compared to that of ZnO nanoparticles prepared using *S. chirayita* and *P. guajava*. Furthermore, an increase in the concentration of the analytes resulted in a tangential increase in the response of the ZnO nanoparticles to the DPPH. At higher concentration of 20 mg mL^{-1} the prepared ZnO nanoparticles show very high degree of antioxidant activity (55.42, 37.44, and 23.17 for ZnO^{Ta}, ZNO^{Sc} and ZnO^{Pg} respectively), whereas the low concentration at 5 mg mL^{-1} resulted in free radical scavenging of only about 13.19, 9.31 and 4.67 for ZnO^{Ta}, ZNO^{Sc} and ZnO^{Pg} respectively, suggesting that the antioxidant property is highly dose dependent. The mechanistic representation of interactions of prepared ZnO nanoparticles with DPPH free radical to form stable DPPH molecule is shown in Fig. S4 and Table S3.

The aforementioned scenario of ZnO^{Ta} showing higher antioxidant activity compared to other counterparts might be due to the smaller particle and crystal size resulting in increased electronic defects leading to more oxygen electron transfer to DPPH. This transition of n π * leads to a decrease in the transition energy, i.e., formation of more stable complex of DPPH molecule [67,72,73]. A similar effect is seen in other metal oxide such as copper oxide nanoparticle whose photocatalytic kinetics is dependent on the surface ionic defects [74]. Briefly, it is suggested that antioxidant activity can be exploited in terms of electron hole pair, i.e., good ratio of defects can lead to increased hydrogen donation capacity which in turn ushers to better redox potential that helps in splitting of water into its radicals [34]. Moreover, the DPPH assessment is in line with the PL assessment, i.e., the ZnO prepared using *T. arjuna* shows higher defects suggesting antioxidant activity can be affected by changes in phytochemicals.

3.3. In-vivo toxicity

To evaluate ZnO nanoparticles (ZnO^{Ta}, ZnO^{Sc} and ZnO^{Pg}) as a potential drug in human body, developmental toxicity was investigated against *D. rerio* embryos. Table 1 shows the toxicity of the prepared ZnO nanoparticles on the *Danio rerio* embryo in terms of their mortality up to 72 h. Among the five different concentrations, 25 and 50 μg mL^{-1} caused least mortality amongst *Danio rerio* embryos inferring high biocompatibility at low concentration of ZnO nanoparticles. Furthermore, the toxicologic effect increased with respect to concentration, i.e., higher mortality of *Danio rerio* embryos occurred at higher concentration, which is in line with a previous study [48].

Interestingly, the mortality of *Danio rerio* during the last 24 h, i.e., at 72 h was phenomenally higher than that at 48 h of exposure to ZnO nanoparticles. This can be attributed to the fact that after 48 h, most of the embryos had been hatched inferring that in the early developmental stages of fish embryos toxicologic effect of ZnO is extremely low. On the other hand, in hatched larvae the toxicological effect of ZnO nanoparticles is quite adverse due to the easy penetration of the nanoparticles into the larvae [25,48].

The prepared ZnO nanoparticles synthesised using the *T. arjuna* showed lower toxic activity compared to the other two nanoparticles. This might be due to the fact that the ZnO synthesised using the *T. arjuna*, due to its lower particle size and higher surface area, resulted in more stability with lower adverse effect to the embryos of zebra fish. When comparing the assessment among other reports, the prepared nanoparticles in this study show lower toxicity and better biocompatibility for biomedicine and implant application [75].

3.4. Measurement of intracellular ROS

To draw a correlation between the intracellular ROS formation inside the cell and the tuneability of ZnO nanoparticles based on the phytochemicals used, intracellular ROS production was estimated. Fig. 5a

Table 1
In-vitro toxicity of the *Danio rerio* treated with prepared ZnO nanoparticles.

Nanoparticles	Concentration (μg mL^{-1})	Mortality %		
		24 h	48 h	72 h
ZnO^{Ta}	Control	0	0	0
	25	0	6.6	6.6
	50	0	6.6	6.6
	75	0	6.6	13.3
	100	0	13.3	13.3
	200	0	13.3	26.6
ZnO^{Sc}	Control	0	0	0
	25	0	6.6	13.3
	50	0	6.6	26.6
	75	0	13.3	40
	100	0	13.3	40
	200	0	26.6	40
ZnO^{Pg}	Control	0	0	0
	25	0	13.3	40
	50	0	13.3	40
	75	0	26.6	40
	100	0	26.6	53.3
	200	0	26.6	53.3

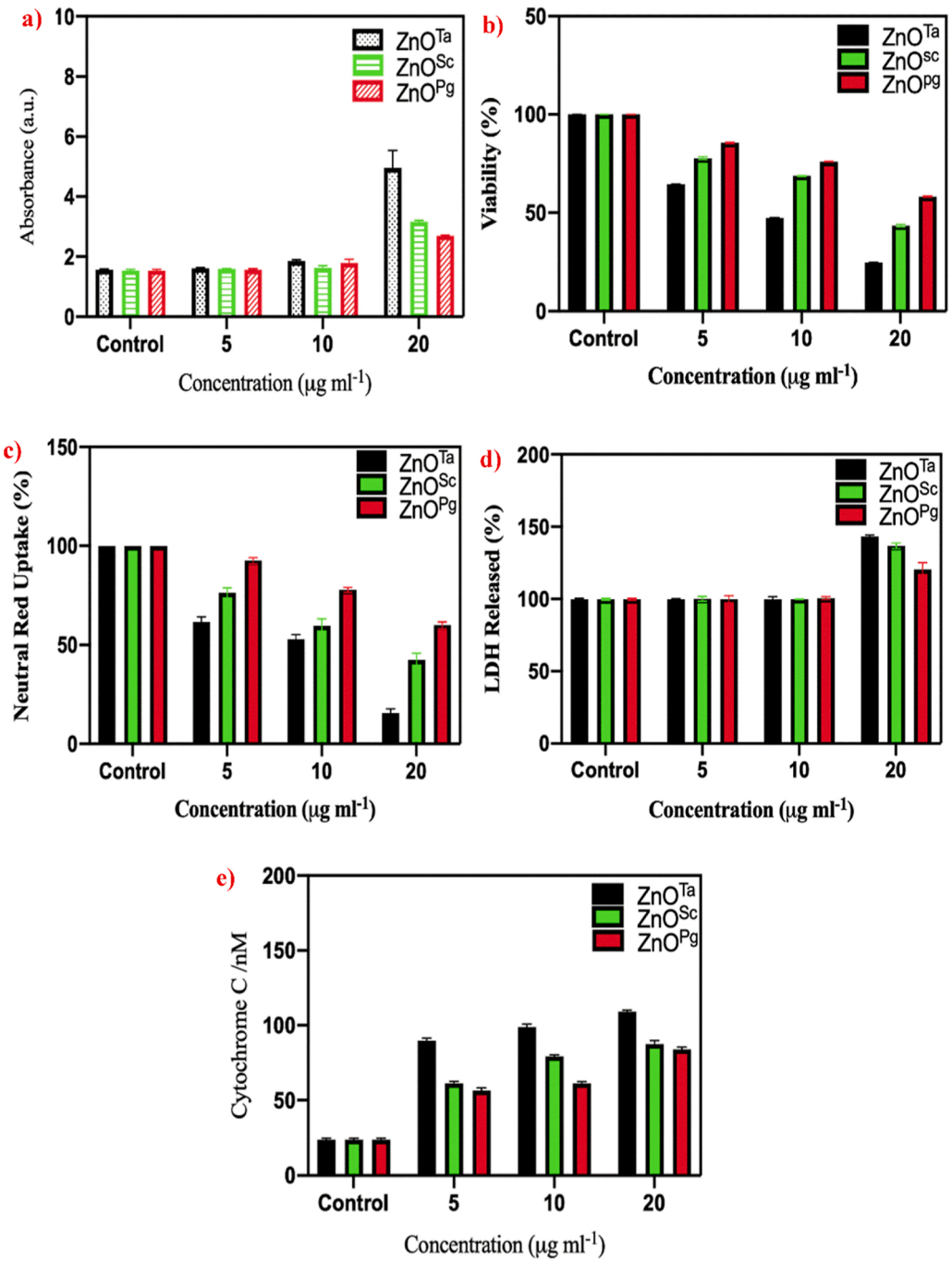

Fig. 5. The comparative in-vitro assessments of various ZnO nanoparticles in terms of concentration and time of treatment: a) Intracellular reactive oxygen species generation; b), c) & d) Cell viability assay using MTT tetrazolium, Neutral red uptake and lactate dehydrogenase release respectively; e) Cytochrome C assay.

shows the amount of intracellular ROS formation inside the ZnO exposed MCF-7 cell with respect to the phytochemicals used (*T. arjuna, S. chirayita,* and *P. guajava*). The high absorbance intensity promulgates to inferring high DCFDA dye suggesting higher ROS generation inside the cell. Furthermore, it was observed from Fig. 5a and Table S4 that the intracellular ROS generation increases (5.562, 3.196, and 2.718 for ZnO^{Ta}, ZnO^{Sc} and ZnO^{Pg} respectively) at higher concentration (20 μg mL^{-1}) of ZnO nanoparticles exposure to MCF-7 cells. These results suggest that intracellular ROS is a nanoparticle dose dependent attribute.

The results also suggest that there is a correlation of the intracellular ROS formation and the higher defects, i.e., the higher number of electrons and holes leads to the formation of super oxide anion and hydroxyl radicals which are both ROS species and can be toxic in nature. A study on ZnO doped with TiO_2 showed a similar ROS production trend suggesting a similar hypothesis, i.e., higher concentration of the metal oxide leads to increased ROS production which in turn causes higher anticancer activity [34]. The ZnO^{Ta} shows higher intracellular ROS formation in the MCF-7 cells (142 ± 0.9) than that of its counterparts (128 ± 0.7, and 121 ± 0.8), as ZnO^{Ta} shows smaller particle size and higher defects, which is in line with the results seen in antioxidant assessment. Furthermore, the spontaneous ROS generation over the surface of the ZnO nanoparticles can be linked to the chemicals and surface characteristics of the nanoparticles [73]. In an earlier study on ZnO nanoparticles and their effects on antibacterial cells, the authors hypothesised the mechanism of surface defect induced ROS generation

which suggested that surface ionic defects can lead to ready reaction with water present inside the cell to give superoxide, hydroxyl radicals as primary ROS products, and in subsequent reaction mechanisms can produce ROS [35]. This ROS generation over the surface of the ZnO nanoparticles can further lead to the generation of free radical after their interaction with the intracellular components [76].

The PL assessment concludes that the ZnO^{Ta} sample showing a high amount of crystal defects correlated to ROS species production inside the cell. Furthermore, it can be hypothesised that the electron-hole pair contributed to the production of intracellular ROS due to the fact that the electron hole pairs formed inside the defects can interact with the oxygen and hydroxyl ions present in the aqueous environment resulting in the formation of superoxide anion from electrons and hydroxyl radical formation from holes. When these radicals interact with the intracellular chemical species, they were reduced to smaller molecules resulting in oxidative stress inside cell [73,76]. Hence the study also suggests a possibility of exploiting nanoparticle physicochemical property to influence biochemical activity.

3.5. Cytotoxicity assay

Cytotoxicity assay is performed to assess how toxic a material is to the cells, whereas for our study we tried to perform the cytotoxicity assay for not only to understand the toxicity of the material but also to assess and define the pathway the cells have taken for cell death, i.e., necrosis or apoptosis. To assess the pathways, ZnO nanoparticles exposed MCF-7 were evaluated with various cell viability assay.

3.5.1. MTT assay

The viability of the MCF-7 cells exposed to ZnO nanoparticles based on viable mitochondria was evaluated using MTT assay. The mechanistic representation of MTT reduction to formazan is shown in Fig. S5. As seen from Fig. 5b, the cells exposed to all the ZnO nanoparticle samples (ZnO^{Ta}, ZnO^{Sc} and ZnO^{Pg}) showed a reduction in percentage cell viability, suggesting that the breast cancer cells upon exposure to the prepared ZnO nanoparticles experienced mitochondrial damage or cell death [76,77]. From the prior assessments it can be inferred that the reduced particle size of the prepared ZnO nanoparticles had led to a greater number of particles entering the cells resulting in higher oxidative stress leading to cellular apoptosis [47,48]. However, at low concentration of 5 μg mL^{-1} there is still high % cell viability (64.48%, 78.04% and 85.35% for ZnO^{Ta}, ZnO^{Sc} and ZnO^{Pg} respectively), whereas there is a significant decrease of cell viability at high concentration (20 μg mL^{-1}) (24.81%, 43.97%, and 58.63% for ZnO^{Ta}, ZnO^{Sc} and ZnO^{Pg} respectively) (Fig. 5b) proving its dose dependent cytotoxic activity. In a previous study on cell viability of MCF-7 and A549 cancer cells using Ag nanoparticles (AgNPs), the authors showed that an increase in AgNPs concentration led to a decrease in cell viability, suggesting the higher AgNPs concentration the higher is anticancer activity [32].

Treatment of ZnO^{Ta} had resulted in lower % MTT inferring higher cell death than that of ZnO^{Sc} and ZnO^{Pg}. It is due to the fact ZnO^{Ta} had smaller leading to higher penetration into the cells. Furthermore, the high surface defects led to higher spontaneous ROS generation over the surface of the ZnO nanoparticles leading to genetic damage causing higher cell deaths [76].

3.5.2. Neutral red uptake assay

For this study, Neutral red uptake indicates cell viability with relation to lysosome [76,78]. As shown in Fig. 5c the NRU assessment suggests that the ZnO nanoparticles cytotoxicity towards MCF-7 changes with respect to both time and dose. Interestingly, the NRU result is similar to that of MTT assay. The nanoparticle cytotoxicity towards cell may be because of intracellular accumulation leading to ROS generation which in turn results in apoptosis or necrosis [76,78]. Mechanistic representation of NRU assay is shown in Fig. S6.

To bring out a relative merit among the ZnO samples (ZnO^{Ta}, ZnO^{Sc} and ZnO^{Pg}) they were also comparatively analysed. ZnO^{Ta} exposed MCF-7 showed lower % NRU absorbed inferring higher cell death of MCF-7 cells in comparison to that of ZnO^{Sc} and ZnO^{Pg} exposed MCF-7 cells. This could be attributed to the ZnO^{Ta} smaller particle size, higher surface area and higher amount of defect, resulting in higher intracellular ROS production causing higher cell death [76,79]. This assessment also suggests that ZnO^{Ta} is a more potential candidate for anticancer drug, in which the cytotoxic activity can be tailored by changing the phytochemicals used during the preparation of ZnO nanoparticles.

3.5.3. LDH release assay

Lactate dehydrogenase (LDH) release assay is also a type of cytotoxic assessment, where cell membrane damage is assessed for the cell death by evaluating the release of the LDH in the testing medium [80]. Comparing to the prior cytotoxic assessment such as MTT, and NRU assay, interesting observations could be made for LDH assay. Fig. 5d shows that at low concentration of ZnO samples no LDH was released. However, at very high concentration the LDH was released into the culture medium. This might be due to instability in the membrane resulting in destabilisation of membrane integrity which can only be achieved at very high concentration of ZnO nanoparticle exposure. This destabilisation of the membrane leads to LDH release which catalyses the conversion of NADP to NADPH and lactate to pyruvate [76,80]. In a comparative assessment, ZnO^{Ta} shows higher cytotoxicity comparing to that of the other two nanoparticles, and this can be ascribed to the smaller particle size and higher defects in the ZnO leading to production of higher ROS over the nanoparticles which in turn results in higher oxidative stress inside the MCF-7 cell. This suggests that ZnO exposure leads to mitochondrial and lysosome damage-based cell death (apoptosis) rather than destabilisation of membrane integrity (necrosis). However, at higher concentration an increased ROS production inside cell can trigger possible necrosis in MCF-7. The mechanistic pathway of LDH releases is shown in Fig. S7.

From the aforementioned cytotoxicity assessments, it can be seen that the ZnO nanoparticles can be used as a potential drug against MCF-7 breast cancer cell line. The above findings also infer that the exploitable cytotoxic activity of ZnO nanoparticles to induce apoptosis in the cell is highly time dependent as well as dose dependent as concluded by MTT and NRU assay. This is also in line with other bio-engineered nanoparticles such as NiO which also tends to show lipid peroxidation at higher concentration [33]. Interestingly, very high concentration of analytes causes the loss of membrane integrity of the cells, i.e., necrosis. This peculiar change in the cell death pathway might have occurred due to an increased accumulation of ZnO nanoparticles causing high oxidative stress inside the cells [76]. The cytotoxic effect of the ZnO nanoparticles prepared from *T. arjuna* it was very high compared to that of the ZnO nanoparticles prepared from the *S. chirayita* and *P. guajava.* This result corresponds to the fact that the ZnO^{Ta} higher structural defects caused the formation of more intracellular ROS resulting in higher oxidative stress inside the cell which in turn causes the cell death.

3.6. Cytochrome c release assay

Cytochrome c release from the mitochondrial inner membrane to the cytosol is one of the characteristic apoptotic biomarkers [81]. To confirm that the treatment with prepared ZnO nanoparticles triggers MCF-7 apoptosis, the analytes were assessed in terms of dose dependency (0, 5, 10, and 20 μg mL^{-1}). Fig. 5e clearly shows that the Cyt-C release increases tangentially with an increase in dose. Moreover, ZnO^{Ta} in line with prior assessment showed higher cytochrome c release compared to other counterparts. The reduced size and increased electronic defects influence spontaneous generation of ROS at the surface which interacts with chemical components leading to activation of apoptotic pathway. Furthermore, all the prepared ZnO nanoparticles caused apoptotic pathway activation.

Interestingly, LDH release assay showed that at higher nanoparticles concentration, membrane destabilisation occurred, a common scenario of necrosis, whereas the cytochrome c release assay confirms that all nanoparticles showed apoptosis. This peculiar phenomenon can be correlated to the fact that even necrosis can occur at higher concentration of nanoparticles if there is an increased ROS production.

3.7. Genotoxic assay

Molecular toxicological assay for DNA, i.e., comet assay was carried out to demonstrate the relation and interaction between the ZnO nanoparticles exposure and genotoxicty in the MCF-7 breast cancer cell line. Genotoxic assessments of the ZnO nanoparticles were performed because the cytotoxic assessment of the ZnO nanoparticles on the MCF-7 cells hinted that the cells might have gone through apoptosis which could have been caused by genetic damage. It was also performed to bring out a correlation between the prepared ZnO nanoparticles and genotoxicity.

Fig. 6 shows the comparative comet assay results performed on the MCF-7 breast cancer cells exposed to various concentrations (0, 5, 10, and 20 μg mL^{-1}) of prepared ZnO nanoparticles (ZnO^{Ta}, ZnO^{Sc} and ZnO^{Pg}). In comparison to the control all the other concentrations of ZnO nanoparticles caused significant damage in genomic DNA of MCF-7 cancer cells. Furthermore, the disruption increased with the concentration inferring that the higher concentration of ZnO nanoparticles used the higher is DNA damage in the MCF-7 cells [76].

The genotoxic result for the ZnO^{Ta} showed more distortion and higher tail formation in comparison to that for the ZnO^{Sc} and ZnO^{Pg}. This high genotoxicity shown by ZnO^{Ta} might be due to the fact that nanoparticles can lead to spontaneous ROS generation at their surface owing to their chemical and surface characteristics, i.e., smaller particle size and higher defect presence, which in turn lead to the production of free radicals after their interaction with the MCF-7 s cellular components such as mitochondrial damage [48,76,82]. Furthermore, it is suggested that oxidation and reduction of the cellular DNA to smaller macromolecules due to the production of these highly reactive free radical can lead to effective cellular apoptosis [80]. Our assessment not only connects the relation between the interaction of the ZnO nanoparticles with the genomic material of the MCF-7 breast cancer cells, but also suggests that the ZnO exposed cells might have gone through

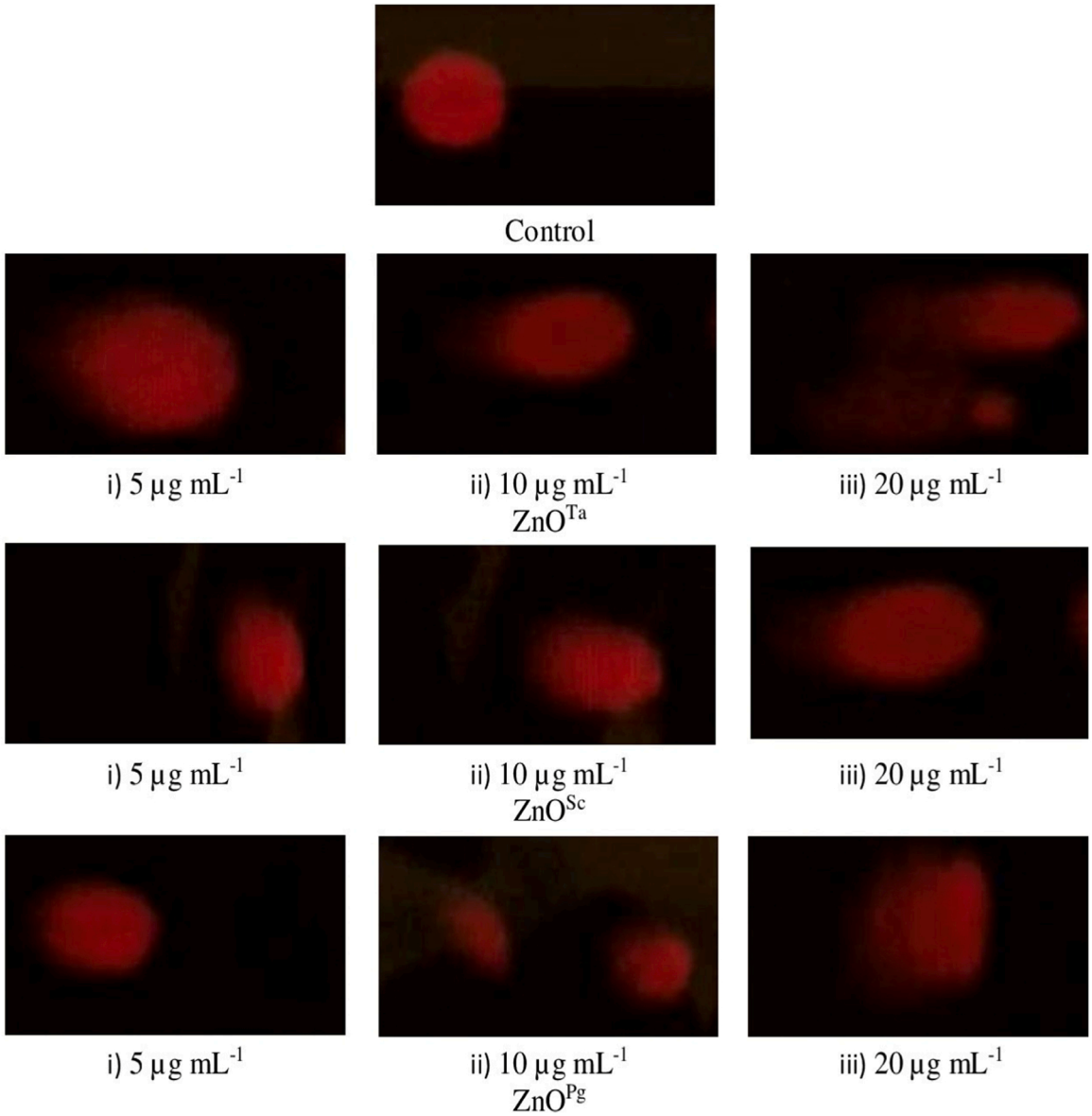

Fig. 6. The genotoxicity of different concentrations of the prepared ZnO nanoparticles analytes.

apoptosis rather than necrosis as well as linking a correlation between phytochemicals tuneability to genotoxicity.

3.8. Apoptosis

For confirming the apoptotic pathway through this assay, MCF-7 cells exposed to only one specific concentration (20 μg mL^{-1}) of ZnO^{Ta} nanoparticles were studied. For a clear understanding and to point out a mechanistic relation, we targeted MAPK pathway and other proteins such as Bax, Bcl2, P38, p53, NF-κβ and their phosphorylated counterparts, as these proteins are responsible for upregulation or downregulation of caspase cascade which in turn leads to apotic activation [83–85]. Western blot analysis revealed that the treated cells showed no change in JNK and P38 expression, whereas there was an increase in the expression of phosphorylated JNK and phosphorylated P38 when compared to the untreated cells (Fig. 7a). On the other hand, there was no observable change in the expression of ERK and phosphorylated ERK in ZnO exposed MCF-7 cells, suggesting no involvement of ZnO nanoparticles on ERK activation.

The MAPK signalling pathway shows an activation of both JNK as well as P38 suggesting an ROS dependent interaction of JNK and P38 by zinc oxide. Therefore, this assessment also points out to the possibility that upon zinc oxide introduction inside a cell, free radical interacts with cellular components such as mitochondria, resulting in formation of ROS, which triggers mitochondrial damage resulting in apoptosis of MCF-7 cells.

Furthermore, a decrease in the procaspase-9 expression and an appearance of cleavage product at 37 kDa (Fig. 7b) suggest the ZnO nanoparticle plays a crucial role in the activation of caspase 9. Tumour suppression protein showed no significant change in the level of P53, whereas there is an increase in the level of phosphorylated P53. Therefore, from the observation in our study it is likely that ROS formation activates P53 in MCF7 breast cancer cell line during exposure to ZnO nanoparticles. For NF-κβ beta protein expression, there was no modulation in cells when exposed to ZnO nanoparticles. Therefore, NF-κβ cellular pathways cannot be activated due to ZnO induced ROS formation in MCF-7 cells.

The ZnO exposed MCF-7 cells showed an increased Bax protein level, while there was a corresponding decrease in Bcl2 protein expression compared to control sample of MCF-7. From our results, we could propose a mechanistic pathway (The detail is shown in supplementary data) of proteins involved in apoptosis of ZnO exposed MCF-7 cells as shown in Fig. 8. Furthermore, in our study we suggest that the activation of the apoptosis cascade is based on the structural defects which lead to higher reactivity of the metal oxides resulting in an increased ROS production inside the cell [85,86].

3.9. Morphological studies of MCF-7 breast cancer cells

The assessment compares the response of the MCF-7 cells without the exposure to ZnO nanoparticles and with exposure to ZnO^{Ta} nanoparticles with various concentrations (5, 10, and 20 μg mL^{-1}). Fig. 9 shows the morphological changes of selected cancer cells in the absence and presence of ZnO at various concentrations. The control cells did not

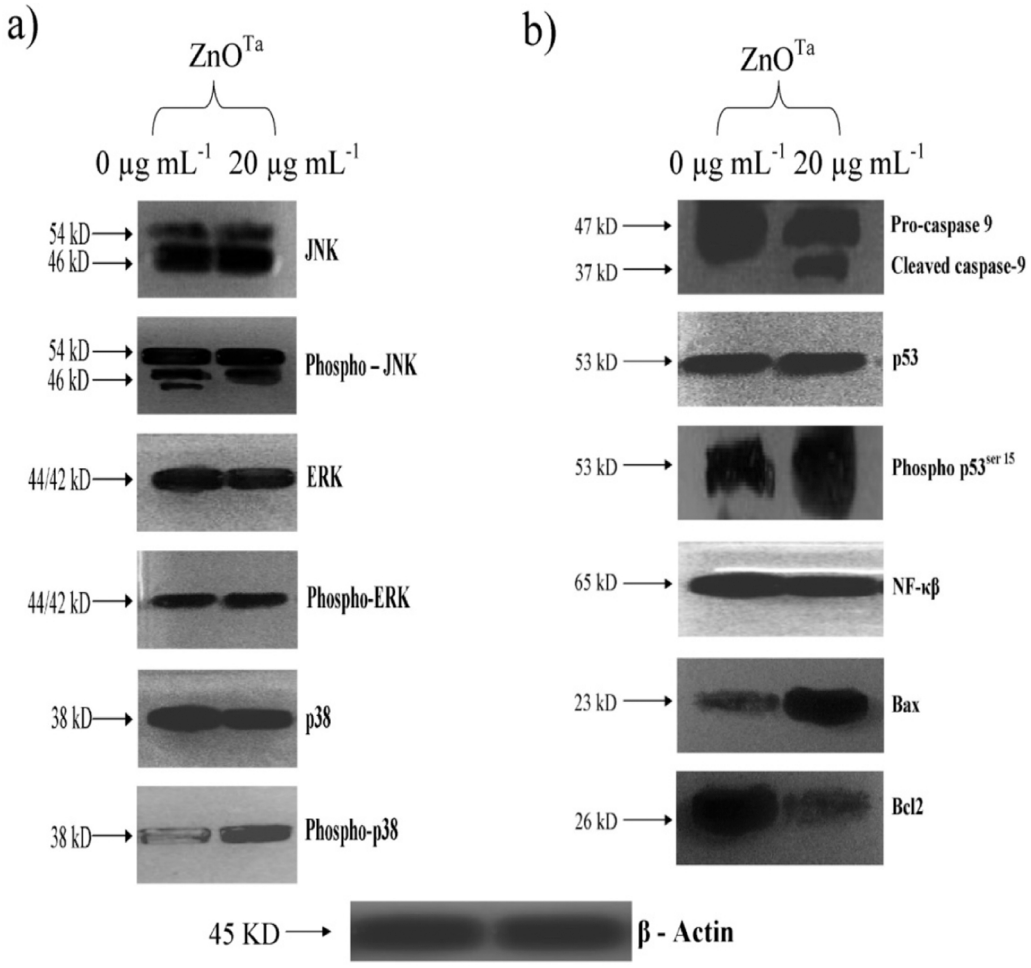

Fig. 7. Western blotting analysis of proteins involved in a) MAPK signalling, b) apoptotic protein signalling in MCF-7 human breast cancer cells. β-Actin was used as internal control to normalise the data.

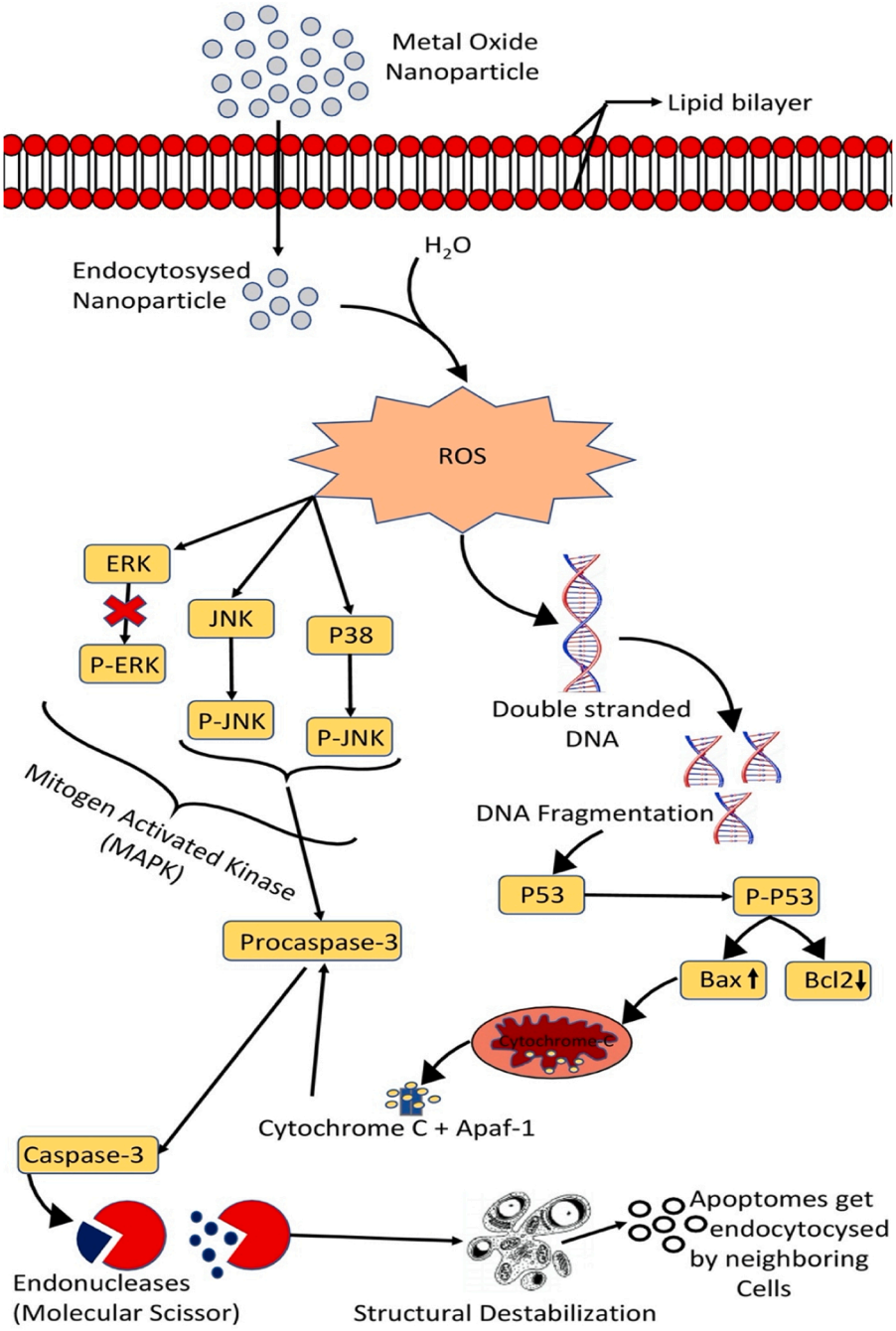

Fig. 8. Proposed mechanisms involved in cellular apoptosis following ZnO nanoparticles intervention.

show any remarkable changes on their morphology, whereas the cells showed cell shrinkage and, membrane bubbling in a dose-dependent manner in the presence of the prepared ZnO.

The assessment confirms the inference that cytological investigations elucidate the antiproliferative effect through membrane bubbling, membrane instability and distressing the cytoskeleton of the cells by the prepared ZnO nanoparticles. This instability of the cell membrane is seen only at higher concentrations of ZnO^{Ta} nanoparticles as confirmed with prior assessments by LDH assay. Moreover, the electron-hole pair in the ZnO nanoparticles results in the formation of superoxide anion (O_2^-) (due to unbalanced electrons) and hydroxyl radical (due to the unbalanced holes) causing cell damage [76,80]. This ROS formation at high level leads to disability of the cell membrane integrity causing necrosis as shown in the prior cytotoxic, as well as oxidative stress parameter assessment.

Upon a comparative evaluation of our results of ZnO treatment on MCF-7 cells with those of other studies on ZnO against MCF-10A (noncarcinogenic breast epithelial cells), it is clear that at lower concentrations no apoptotic activation was observed, whereas above a threshold concentration apoptosis can be activated. In cancer cells, the genetic material and protein structure due to its epigenetic modification can readily attach to the ROS leading to downregulation or upregulation of some cancer related proteins as shown in Fig. 7. Moreover, the in-vitro study performed in this study supports the aforementioned trait, i.e., only at very high concentration, ZnO nanoparticles are cytotoxic. Thus, our study not only tries to demonstrate a detailed assessment of the ZnO nanoparticle interaction at subcellular level, but also points out its pharmacological potential in modern clinical anticancer therapeutics.

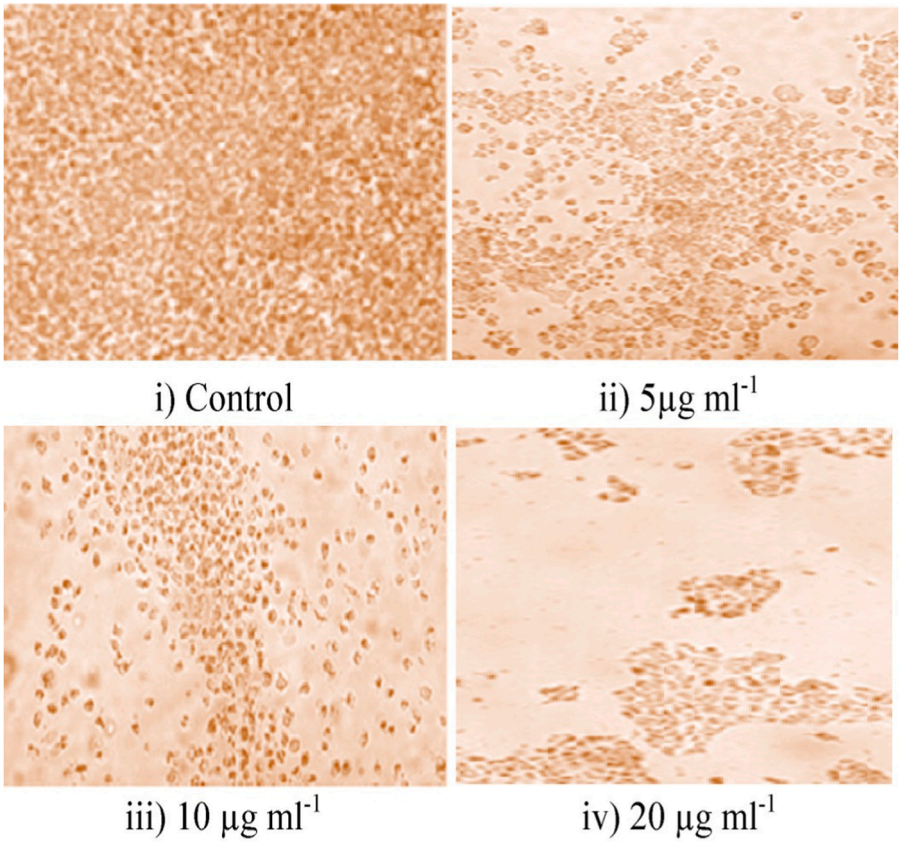

Fig. 9. Morphological assessment of MCF-7 human breast cancer cells treated with different concentrations of ZnO nanoparticles prepared from plant extract of *Terminalia arjuna.*

4. Conclusion

ZnO nanoparticles with poly crystalline wurtzite structure are synthesised by employing hydrothermal method using the extract of *Terminalia arjuna, Swertia chiratiya,* and *Psidium guajava.* The study successfully revealed the change in physicochemical property of the ZnO nanoparticle with change in active reducing agent during its synthesis and tried to correlate the physicochemical properties to biological activities such as cyto-toxicity against *Danio rerio* and anticancer activity against MCF-7 cells. Nanoparticles with smaller particle size, higher surface area, and structural defects can lead to increased spontaneous ROS generation which in turn can activate apoptotic pathway. Most importantly, ZnO nanoparticle is toxic and causes oxidative stress induced apoptosis in MCF-7 cells which can be used as a potential anticancer drug.

CRediT authorship contribution statement

Raunak Saha: Conceptualization, Methodology, Investigation, Writing – original draft. **Karthik Subramani:** Conceptualization, Methodology, Investigation, Writing – original draft. **Sreenath Dey:** Investigation. **Saheri Sikdar:** Investigation. **Aran Incharoensakdi:** Conceptualization, Supervision, Funding acquisition, Project administration, Writing – review & editing.

Conflicts of interest

The authors declare no conflicts of interest.

Data availability

Data will be made available on request.

Acknowledgements

The authors acknowledge the Second Century Fund (C2F), Chulalongkorn University, Bangkok, Thailand. One of the authors Dr. Karthik Subramani is grateful to the second century fund (C2F) for providing the Postdoctoral fellowship. A.I. acknowledges the research grants from CU Ratchadaphiseksomphot Endowment Fund (CU_GR 62_88_23_33) and from Thailand Research Fund (IRG5780008).

Appendix A. Supplementary material

Supplementary data associated with this article can be found in the online version at doi:10.1016/j.procbio.2023.03.016.

References

[1] R. Vakayil, S. Muruganantham, N. Kabeerdass, M. Rajendran, A. Mahadeopalve, S. Ramasamy, T.A. Alahmadi, H.S. Almoallim, V. Manikandan, M. Mathanmohun, *Acorus calamus*-zinc oxide nanoparticle coated cotton fabrics shows antimicrobial and cytotoxic activities against skin cancer cells, Process Biochem. 111 (1) (2021) 1–8, https://doi.org/10.1016/j.procbio.2021.08.024.
[2] O.E. Omoike, R.P. Pack, H.M. Mamudu, Y. Liu, L. Wang, A cross-sectional study of the association between perfluorinated chemical exposure and cancers related to deregulation of estrogen receptors, Environ. Res. 196 (2021), 110329, https://doi.org/10.1016/j.envres.2020.110329.
[3] E.J. Calabrese, P.B. Selby, Cover up and cancer risk assessment: prominent US scientists suppressed evidence to promote adoption of LNT, Environ. Res. 210 (2022), 112973, https://doi.org/10.1016/j.envres.2022.112973.
[4] S.M. Mutuku, X. Spotbeen, P.J. Trim, M.F. Snel, L.M. Butler, J.V. Swinnen, Unravelling prostate cancer heterogeneity using spatial approaches to lipidomics

and transcriptomics, Cancers 14 (2022) 1702, https://doi.org/10.3390/cancers14071702.
[5] U. Mehraj, U. Mushtaq, M.A. Mir, A. Saleem, M.A. Macha, M.N. Lone, A. Hamid, M. A. Zargar, S.M. Ahmad, N.A. Wani, Chemokines in triple-negative breast cancer heterogeneity: new challenges for clinical implications, in: Seminars in Cancer Biology, Elsevier, 2022, https://doi.org/10.1016/j.semcancer.2022.03.008.
[6] S. Mirzaei, M.H. Gholami, A. Zabolian, H. Saleki, M.V. Farahani, S. Hamzehlou, F. B. Far, S.O. Sharifzadeh, S. Samarghandian, H. Khan, Caffeic acid and its derivatives as potential modulators of oncogenic molecular pathways: New hope in the fight against cancer, Pharmacol. Res. 171 (2021), 105759, https://doi.org/10.1016/j.phrs.2021.105759.
[7] X. Liu, X. Wang, S. Ye, R. Li, H. Li, A one–two–three multifunctional system for enhanced imaging and detection of intracellular MicroRNA and chemogene therapy, ACS Appl. Mater. Interface 13 (2021) 27825–27835, https://doi.org/10.1021/acsami.1c04353.
[8] P.P. Reis, W.L. Lam, D. Elgui de Oliveira, Human and oncoviral non-coding rnas as modulators of cancer aggressiveness and disease progression, Front. Med. (2021), 641725, https://doi.org/10.3389/fonc.2020.641725.
[9] C. Ramin, D.R. Withrow, B.C. Davis Lynn, G.L. Gierach, A. Berrington de González, Risk of contralateral breast cancer according to first breast cancer characteristics among women in the USA, 1992–2016, Breast Cancer Res. 23 (2021) 1–10, https://doi.org/10.1186/s13058-021-01400-3.
[10] J. Anitha, R. Selvakumar, K. Murugan, Chitosan capped ZnO nanoparticles with cell specific apoptosis induction through P53 activation and G2/M arrest in breast cancer cells – in vitro approaches, Int. J. Biol. Macromol. 136 (2019) 686–696, https://doi.org/10.1016/j.ijbiomac.2019.05.217.
[11] P. Thakur, K. Baraskar, V.K. Shrivastava, Histopathological characteristics: breast cancer subtypes depending on receptor status, clinical and pathological staging of breast cancer, Breast Cancer: from Bench to Personalized Medicine, Springer, 2022, pp. 31–46. ⟨https://doi.org/10.1007/978-981-19-0197-3_2⟩.
[12] X. Fang, J. Cao, A. Shen, Advances in anti-breast cancer drugs and the application of nano-drug delivery systems in breast cancer therapy, J. Drug Deliv. Sci. Technol. 57 (2020), 101662, https://doi.org/10.1016/j.jddst.2020.101662.
[13] M.S. Hossain, H. Karuniawati, A.A. Jairoun, Z. Urbi, D.J. Ooi, A. John, Y.C. Lim, K. K. Kibria, A. Mohiuddin, L.C. Ming, Colorectal cancer: a review of carcinogenesis, global epidemiology, current challenges, risk factors, preventive and treatment strategies, Cancers 14 (2022) 1732, https://doi.org/10.3390/cancers14071732.
[14] V. Ravichandran, Q.T. Hoang, T.G.N. Cao, M.S. Shim, Glutathione-depleted and cancer-targeted nanocapsules encapsulating bimetallic oxide nanoparticles for enhanced chemo-sonodynamic therapy, J. Ind. Eng. Chem. 114 (2022) 171–180, https://doi.org/10.1016/j.jiec.2022.07.007.
[15] S. Dasari, S. Njiki, A. Mbemi, C.G. Yedjou, P.B. Tchounwou, Pharmacological effects of cisplatin combination with natural products in cancer chemotherapy, Int. J. Mol. Sci. 23 (2022) 1532, https://doi.org/10.3390/ijms23031532.
[16] P.M. Forde, J. Spicer, S. Lu, M. Provencio, T. Mitsudomi, M.M. Awad, E. Felip, S. R. Broderick, J.R. Brahmer, S.J. Swanson, et al., Neoadjuvant nivolumab plus chemotherapy in resectable lung cancer, N. Engl. J. Med. 386 (2022) 1973–1985, https://doi.org/10.1056/NEJMoa220217.
[17] N. Lv, X. Zhang, S. Wang, Y. Wu, X. Ge, J. Song, Q. Ma, S. Gao, Stimuli-responsive hybrid vesicle for tumor dual-model NIR-II photoacoustic and fluorescence imaging and precise radiotherapy, Adv. Opt. Mater., 2200694, ⟨https://doi.org/10.1002/adom.202200694⟩.
[18] G. Petroni, L.C. Cantley, L. Santambrogio, S.C. Formenti, L. Galluzzi, Radiotherapy as a tool to elicit clinically actionable signalling pathways in cancer, Nat. Rev. Clin. Oncol. 19 (2022) 114–131, https://doi.org/10.1038/s41571-021-00579-w.
[19] J. Li, L. Xie, W. Sang, W. Li, G. Wang, J. Yan, Z. Zhang, H. Tian, Q. Fan, Y. Dai, A Metal-phenolic nanosensitizer performs hydrogen sulfide-reprogrammed oxygen metabolism for cancer radiotherapy intensification and immunogenicity, Angew. Chem. Int. Ed. 61 (2022), e202200830, https://doi.org/10.1002/anie.202200830.
[20] M.D. Vesely, T. Zhang, L. Chen, Resistance mechanisms to anti-PD cancer immunotherapy, Annu. Rev. Immunol. 40 (2022) 45–74, https://doi.org/10.1146/annurev-immunol-070621-030155.
[21] W. Fu, C. Lei, C. Wang, Z. Ma, T. Li, F. Lin, R. Mao, J. Zhao, S. Hu, Synthetic libraries of immune cells displaying a diverse repertoire of chimaeric antigen receptors as a potent cancer immunotherapy, Nat. Biomed. Eng. (2022) 1–13, https://doi.org/10.1038/s41551-022-00895-1.
[22] Z. Sayyar, H.J. Malmiri, N. Beheshtizadeh, A study on the anticancer and antimicrobial activity of curcumin nanodispersion and synthesized ZnO nanoparticles, Process Biochem. 121 (2022) 18–25, https://doi.org/10.1016/j.procbio.2022.06.033.
[23] S.A.S. Shandiz, F. Sharifian, S. Behboodi, F. Ghodratpour, F. Baghbani-Arani, Evaluation of metastasis suppressor genes expression and in vitro anti-cancer effects of zinc oxide nanoparticles in human breast cancer cell lines MCF-7 and T47D, Avicenna J. Med. Biotechnol. 13 (2021) 9, https://doi.org/10.18502/ajmb.v13i1.4576.
[24] C. Wen, L. Wang, L. Liu, X.C. Shen, H. Chen, Surface-enhanced raman probes based on gold nanomaterials for in vivo diagnosis and imaging, e202200014, Chem. Asian J. 17 (2022), https://doi.org/10.1002/asia.202200014.
[25] C. Sheng, B. Wu, L. Li, Y. Zhao, Merging DNA probes with nanotechnology for rna imaging in vivo, Curr. Anal. Chem. 18 (2022) 622–629, https://doi.org/10.2174/1573411017666210211093534.
[26] G. Si, S. Hapuarachchige, D. Artemov, Ultrasmall superparamagnetic iron oxide nanoparticles as nanocarriers for magnetic resonance imaging: development and in vivo characterization, ACS Appl. Nano Mater. 5 (2022) 9625–9632, https://doi.org/10.1021/acsanm.2c01835.
[27] S.I. Kaya, G. Ozcelikay, F. Mollarasouli, N.K. Bakirhan, S.A. Ozkan, Recent achievements and challenges on nanomaterial based electrochemical biosensors for the detection of colon and lung cancer biomarkers, Sens. Actuators B Chem. 351 (2022), 130856, https://doi.org/10.1016/j.snb.2021.130856.
[28] F.A. Al-Joufi, A. Setia, M.M. Salem-Bekhit, R.K. Sahu, F.Y. Alqahtani, R. Widyowati, F.S. Aleanizy, Molecular pathogenesis of colorectal cancer with an emphasis on recent advances in biomarkers, as well as nanotechnology-based diagnostic and therapeutic approaches, Nanomaterials 12 (2022) 169, https://doi.org/10.3390/nano12010169.
[29] G. Lohiya, D.S. Katti, Carboxylated chitosan-mediated improved efficacy of mesoporous silica nanoparticle-based targeted drug delivery system for breast cancer therapy, Carbohydr. Polym. 277 (2022), 118822, https://doi.org/10.1016/j.carbpol.2021.118822.
[30] S. Chandrasekaran, V. Anbazhagan, S. Anusuya, Green route synthesis of ZnO nanoparticles using Senna auriculata aqueous flower extract as reducing agent and evaluation of its antimicrobial, antidiabetic and cytotoxic activity, Appl. Biochem. Biotechnol. (2022) 1–15, https://doi.org/10.1007/s12010-022-03900-0.
[31] S. Anjum, M. Hashim, S.A. Malik, M. Khan, J.M. Lorenzo, B.H. Abbasi, C. Hano, Recent advances in zinc oxide nanoparticles (Zno nps) for cancer diagnosis, target drug delivery, and treatment, Cancers 13 (2021) 4570, https://doi.org/10.3390/cancers1318457.
[32] K. Venugopal, H.A. Rather, K. Rajagopal, M.P. Shanthi, K. Sheriff, M. Illiyas, R. A. Rather, E. Manikandan, S. Uvarajan, M. Bhaskar, Synthesis of silver nanoparticles (Ag NPs) for anticancer activities (MCF 7 breast and A549 lung cell lines) of the crude extract of Syzygium aromaticum, J. Photochem. Photobiol. B Biol. (2017) 282–289, https://doi.org/10.1016/j.jphotobiol.2016.12.013.
[33] A.A. Ezhilarasi, J.J. Vijaya, K. Kaviyarasu, M. Maaza, A. Ayeshamariam, L. J. Kennedy, Green synthesis of NiO nanoparticles using Moringa oleifera extract and their biomedical applications: cytotoxicity effect of nanoparticles against HT-29 cancer cells, J. Photochem. Photobiol. B Biol. (2016) 352–360, https://doi.org/10.1016/j.jphotobiol.2016.10.00.
[34] K. Kaviyarasu, N. Geetha, K. Kanimozhi, C.M. Magdalane, S. Sivaranjani, A. Ayeshamariam, J. Kennedy, M. Maaza, In vitro cytotoxicity effect and antibacterial performance of human lung epithelial cells A549 activity of zinc oxide doped TiO2 nanocrystals: investigation of bio-medical application by chemical method, Mater. Sci. Eng. C 74 (2017) 325–333, https://doi.org/10.1016/j.msec.2016.12.024.
[35] T.A. Singh, A. Sharma, N. Tejwan, N. Ghosh, J. Das, P.C. Sil, A state of the art review on the synthesis, antibacterial, antioxidant, antidiabetic and tissue regeneration activities of zinc oxide nanoparticles, Adv. Colloid Interface Sci. 295 (2021), 102495, https://doi.org/10.1016/j.cis.2021.102495.
[36] A.T. Khalil, M. Ovais, I. Ullah, M. Ali, Z.K. Shinwari, S. Khamlich, M. Maaza, *Sageretia thea* (Osbeck.) mediated synthesis of zinc oxide nanoparticles and its biological applications, Nanomedicine 15 (2017) 1767–1789, https://doi.org/10.2217/nnm-2017-0124.
[37] M. Henini, F. Ezema, E. Manikandan, J. Kennedy, K. Bouziane, M. Chaker, A. Gibaud, A.K. Haque, Z. Nuru, I. Ahmad, R. Obodo, Peculiar size effects in nanoscaled systems, Nanoscale Horiz. (2022), https://doi.org/10.25159/NanoHorizons.9d53e2220e31.
[38] B.D. Ngom, T. Mpahane, E. Manikandan, M. Maaza, ZnO nano-discs by lyophilization process: size effects on their intrinsic luminescence, 656, J. Alloy. Compd. 656 (2016) 758–763, https://doi.org/10.1016/j.jallcom.2015.09.230.
[39] H. Agarwal, D. Goyal, Photocatalytic degradation of textile dyes using phycosynthesised ZnO nanoparticles, Inorg. Chem. Commun. 142 (2022), 109676, https://doi.org/10.1016/j.inoche.2022.109676.
[40] E.Z. Gomaa, Microbial mediated synthesis of zinc oxide nanoparticles, characterization and multifaceted applications, J. Inorg. Organomet. Polym. Mater. (2022) 1–19, https://doi.org/10.1007/s10904-022-02406-w.
[41] O.R. Abbasabadi, M.R. Farahpour, Z.G. Tabatabaei, Accelerative effect of nanohydrogels based on chitosan/ZnO incorporated with citral to heal the infected full-thickness wounds; an experimental study, Int. J. Biol. Macromol. 217 (2022) 42–54, https://doi.org/10.1016/j.ijbiomac.2022.07.038.
[42] I.M. Hasan, A.R. Tawfik, F.H. Assaf, GC/MS screening of buckthorn phytochemicals and their use to synthesize ZnO nanoparticles for photocatalytic degradation of malachite green dye in water, Water Sci. Technol. 85 (2022) 664–684, https://doi.org/10.2166/wst.2021.638.
[43] K. Parveen, N. Kumar, D. Sharma, L. Ledwani, Evaluation of efficacy of "*cassia renigera*" leaf extract mediated zno nanoparticles as nano fertilizer for cauliflower plant, ChemistrySelect 7 (2022), e202200367, https://doi.org/10.1002/slct.202200367.
[44] G.T. Anand, D. Renuka, R. Ramesh, L. Anandaraj, S.J. Sundaram, G. Ramalingam, C.M. Magdalane, A.K. Bashir, M. Maaza, K. Kaviyarasu, Green synthesis of ZnO nanoparticle using Prunus dulcis (Almond Gum) for antimicrobial and supercapacitor applications, Surf. Interfaces, 17, 2019, 100376. ⟨https://doi.org/10.1016/j.surfin.2019.100376⟩.
[45] V. Krishnan, G. Bupesh, E. Manikandan, A.K. Thanigai, S. Magesh, R. Kalyanaraman, M. Maaza, Green synthesis of silver nanoparticles using *Piper nigrum* concoction and its anticancer activity against MCF-7 and Hep-2 cell lines, 2472-1212, J. Antimicrob. Agents 3 (2016), https://doi.org/10.4172/2472-1212.1000123.
[46] S. Hameed, A.T. Khalil, M. Ali, M. Numan, S. Khamlich, Z.K. Shinwari, M. Maaza, Greener synthesis of ZnO and Ag–ZnO nanoparticles using *Silybum marianum* for diverse biomedical applications, Nanomedicine 6 (2019) 655–673, https://doi.org/10.2217/nnm-2018-0279.
[47] R. Saha, K. Subramani, S.A.K. Petchi Muthu Raju, S. Rangaraj, R. Venkatachalam, *Psidium guajava* leaf extract-mediated synthesis of ZnO nanoparticles under

different processing parameters for hydrophobic and antibacterial finishing over cotton fabrics, Prog. Org. Coat. 124 (2018) 80–91, https://doi.org/10.1016/j.porgcoat.2018.08.004.
[48] R. Saha, S. Karthik, K.S. Balu, R. Suriyaprabha, P. Siva, V. Rajendran, Influence of the various synthesis methods on the ZnO nanoparticles property made using the bark extract of *Terminalia arjuna*, Mater. Chem. Phys. 209 (2018) 208–216, https://doi.org/10.1016/j.matchemphys.2018.01.023.
[49] R. Saha, K. Subramani, S. Sikdar, K. Fatma, S. Rangaraj, Effects of processing parameters on green synthesised ZnO nanoparticles using stem extract of *Swertia chirayita*, Biocatal. Agric. Biotechnol. 33 (2021), 101968, https://doi.org/10.1016/j.bcab.2021.101968.
[50] K. Marxen, K.H. Vanselow, S. Lippemeier, R. Hintze, A. Ruser, U.P. Hansen, Determination of DPPH radical oxidation caused by methanolic extracts of some microalgal species by linear regression analysis of spectrophotometric measurements, Sensors 7 (2007) 2080–2095, https://doi.org/10.3390/s7102080.
[51] M.R. Embry, S.E. Belanger, T.A. Braunbeck, M. Galay-Burgos, M. Halder, D. E. Hinton, M.A. Léonard, A. Lillicrap, T. Norberg-King, G. Whale, The fish embryo toxicity test as an animal alternative method in hazard and risk assessment and scientific research, Aquat. Toxicol. 97 (2010) 79–87, https://doi.org/10.1016/j.aquatox.2009.12.008.
[52] D. Figueroa, M. Asaduzzaman, F. Young, Real time monitoring and quantification of reactive oxygen species in breast cancer cell line MCF-7 by 2′, 7′–dichlorofluorescin diacetate (DCFDA) assay, J. Pharmacol. Toxicol. Methods 94 (2018) 26–33, https://doi.org/10.1016/j.vascn.2018.03.007.
[53] S.S. Hosseni, H.R. Joshaghani, M. Eskandari, Colorimetric MTT assessment of antifungal activity of ZnO nanowires against candida dubliensis bioflm, Jundishapur Sci. Med. J. 12 (2013) 69–80.
[54] N.N. Farshori, E.S. Al-Sheddi, M.M. Al-Oqail, J. Musarrat, A.A. Al-Khedhairy, M. A. Siddiqui, Anticancer activity of *Petroselinum sativum* seed extracts on MCF-7 human breast cancer cells, Asian Pac. J. Cancer Prev. 10 (2013) 5719–5723, https://doi.org/10.7314/APJCP.2013.14.10.5719.
[55] V. Forest, A. Figarol, D. Boudard, M. Cottier, P. Grosseau, J. Pourchez, Adsorption of lactate dehydrogenase enzyme on carbon nanotubes: how to get accurate results for the cytotoxicity of these nanomaterials, Langmuir 31 (2015) 3635–3643, https://doi.org/10.1021/acs.langmuir.5b00631.
[56] E.I. Cortés-Gutiérrez, F. Hernández-Garza, J.O. García-Pérez, M.I. Dávila-Rodríguez, M.E. Aguado-Barrera, R.M. Cerda-Flores, Evaluation of DNA single and double strand breaks in women with cervical neoplasia based on alkaline and neutral comet assay techniques, J. Biomed. Biotechnol. (2012), https://doi.org/10.1155/2012/385245.
[57] M. Eşmekaya, A.Y. Canseven Kurşun, H. Kayhan, M. Tuysuz, B. Sirav, N. Seyhan, Mitochondrial hyperpolarization and cytochrome-c release in microwave-exposed MCF-7 cells, Gen. Physiol. Biophys. (2017) 36, https://doi.org/10.4149/gpb_2016021.
[58] N.J. Kruger, The Bradford method for protein quantitation. The Protein Protocols Handbook, 2009, pp. 17–24.
[59] C. Mao, Y. Xiang, X. Liu, Z. Cui, X. Yang, K.W.K. Yeung, H. Pan, X. Wang, P.K. Chu, S. Wu, Photo-inspired antibacterial activity and wound healing acceleration by hydrogel embedded with Ag/Ag@ AgCl/ZnO nanostructures, ACS Nano 11 (2017) 9010–9021, https://doi.org/10.1021/acsnano.7b03513.
[60] R. Sharma, N. Saxena, N. Pandey, A. Dawar, S. Ojha, V. Chawla, R. Laishram, R. Krishna, O. Sinha, Mg-doped tailoring of Zinc oxide for UV-photodetection application, Opt. Mater. 125 (2022), 112056, https://doi.org/10.1016/j.optmat.2022.112056.
[61] P. Erhart, K. Albe, Diffusion of zinc vacancies and interstitials in zinc oxide, Appl. Phys. Lett. 88 (2006), 201918, https://doi.org/10.1063/1.2206559.
[62] R. Brayner, R. Ferrari-Iliou, N. Brivois, S. Djediat, M.F. Benedetti, F. Fiévet, Toxicological impact studies based on *Escherichia coli* bacteria in ultrafine ZnO nanoparticles colloidal medium, Nano Lett. 6 (2006) 866–870, https://doi.org/10.1021/nl052326h.
[63] N.S. Kumar, M. Ganapathy, S. Sharmila, M. Shankar, M. Vimalan, I.V. Potheher, ZnO/Ni (OH) 2 core-shell nanoparticles: synthesis, optical, electrical and photoacoustic property analysis, J. Alloy. Compd. 703 (2017) 624–632, https://doi.org/10.1016/j.jallcom.2017.01.323.
[64] F.A. Jan, R. Ullah, N. Ullah, M. Usman, Exploring the environmental and potential therapeutic applications of *Myrtus communis L.* assisted synthesized zinc oxide (ZnO) and iron doped zinc oxide (Fe-ZnO) nanoparticles, J. Saudi Chem. Soc. 25 (2021), 101278, https://doi.org/10.1016/j.jscs.2021.101278.
[65] A. van Dijken, E.A. Meulenkamp, D. Vanmaekelbergh, A. Meijerink, Influence of adsorbed oxygen on the emission properties of nanocrystalline ZnO particles, J. Phys. Chem. B 104 (2000) 4355–4360, https://doi.org/10.1021/jp993998x.
[66] B. Sathyaseelan, E. Manikandan, K. Sivakumar, J. Kennedy, M. Maaza, Enhanced visible photoluminescent and structural properties of ZnO/KIT-6 nanoporous materials for white light emitting diode (w-LED) application, J. Alloy. Com. 651 (2015) 479–482, https://doi.org/10.1016/j.jallcom.2015.08.094.
[67] G. Madhumitha, J. Fowsiya, N. Gupta, A. Kumar, M. Singh, Green synthesis, characterization and antifungal and photocatalytic activity of Pithecellobium dulce peel–mediated ZnO nanoparticles, J. Phys. Chem. Solids 127 (2019) 43–51, https://doi.org/10.1016/j.jpcs.2018.12.005.
[68] A. Rahman, M.H. Harunsani, A.L. Tan, M.M. Khan, Zinc oxide and zinc oxide-based nanostructures: biogenic and phytogenic synthesis, properties and applications, Bioprocess Biosyst. Eng. 44 (2021) 1333–1372, https://doi.org/10.1007/s00449-021-02530-w.
[69] L. Jiang, J. Li, K. Huang, S. Li, Q. Wang, Z. Sun, Z., T. Mei, J. Wang, L. Zhang, N. Wang, X. Wang, Low-temperature and solution-processable zinc oxide transistors for transparent electronics, ACS Omega 12 (2017) 8990–8996, https://doi.org/10.1021/acsomega.7b01420.
[70] S. Yin, E.R. Bernstein, Gas phase chemistry of neutral metal clusters: distribution, reactivity and catalysis, Int. J. Mass Spectrom. 15 (49–65) (2012), https://doi.org/10.1016/j.ijms.2012.06.001.
[71] R. Xu, C. Wu, H. Xu, Particle size and zeta potential of carbon black in liquid media, Carbon 14 (2007) 2806–2809, https://doi.org/10.1016/j.carbon.2007.09.010.
[72] A. Diallo, B. Ngom, E. Park, M. Maaza, Green synthesis of ZnO nanoparticles by *Aspalathus linearis*: structural & optical properties, J. Alloy. Compd. 646 (2015) 425–430, https://doi.org/10.1016/j.jallcom.2015.05.242.
[73] E.N. Danial, M. Hjiri, M.S. Abdel-Wahab, N. Alonizan, L. El Mir, M. Aida, Antibacterial activity of In-doped ZnO nanoparticles, Inorg. Chem. Commun. 122 (2020), 108281, https://doi.org/10.1016/j.inoche.2020.108281.
[74] A.C. Nwanya, L.C. Razanamahandry, A.K. Bashir, C.O. Ikpo, S.C. Nwanya, S. Botha, S.K. Ntwampe, Fl Ezema, E.I. Iwuoha, M. Maaza, Industrial textile effluent treatment and antibacterial effectiveness of *Zea mays L.* Dry husk mediated bio-synthesized copper oxide nanoparticles, J. Hazard. Mater. 375 (2019) 281–289, https://doi.org/10.1016/j.jhazmat.2019.05.004.
[75] S. Rangaraj, R. Venkatachalam, *In vitro* and in vivo characteristics of biogenic high surface silica nanoparticles in A549 lung cancer cell lines and *Danio rerio* model systems for inorganic biomaterials development, Artif. Cells Nanomed. Biotechnol. 46 (2018) 1415–1424, https://doi.org/10.1080/21691401.2017.1369427.
[76] V. Sharma, D. Anderson, A. Dhawan, Zinc oxide nanoparticles induce oxidative DNA damage and ROS-triggered mitochondria mediated apoptosis in human liver cells (HepG2), Apoptosis 17 (2012) 852–870, https://doi.org/10.1007/s10495-012-0705-6.
[77] G. Ates, T. Vanhaecke, V. Rogiers, R.M. Rodrigues, Assaying cellular viability using the neutral red uptake assay, in: Cell Viability Assays, Springer, 2017, pp. 19–26, https://doi.org/10.1007/978-1-4939-6960-9_2.
[78] C. Oliveira, F. Basso, E. Lins, C. Kurachi, J. Hebling, V.S. Bagnato, C. de Souza Costa, In vitro effect of low-level laser on odontoblast-like cells, Laser Phys. Lett. 8 (2010) 155, https://doi.org/10.1002/lapl.201010101.
[79] T.S. Aldeen, H.E. Mohamed HE, M. Maaza, ZnO nanoparticles prepared via a green synthesis approach: Physical properties, photocatalytic and antibacterial activity, J. Phys. Chem. Solids 160 (2022), 110313, https://doi.org/10.1016/j.jpcs.2021.110313.
[80] T. Kang, R. Guan, X. Chen, Y. Song, H. Jiang, J. Zhao, In vitro toxicity of different-sized ZnO nanoparticles in Caco-2 cells, Nanoscale Res. Lett. 8 (2013) 1–8, https://doi.org/10.1186/1556-276X-8-496.
[81] H. Bayir, B. Fadeel, M. Palladino, E. Witasp, I. Kurnikov, Y. Tyurina, V. Tyurin, A. Amoscato, J. Jiang, P. Kochanek, Apoptotic interactions of cytochrome c: redox flirting with anionic phospholipids within and outside of mitochondria, Biochim. Biophys. Acta Bioenerg. 2006 (1757) 648–659, https://doi.org/10.1007/s13273-021-00118-9.
[82] M. Maaza, B.D. Ngom, M. Achouri, K. Manikandan, Functional nanostructured oxides, Vacuum 114 (2015) 172–187, https://doi.org/10.1016/j.vacuum.2014.12.023.
[83] B. Alberts, A. Johnson, J. Lewis, M. Raff, K. Roberts, P. Walter. Molecular Biology of the Cell, Garland Science, New York, USA, 2002. ⟨www.ncbi.nlm.nih.gov/books/NBK21054⟩.
[84] S.W. Lowe, A.W. Lin, Apoptosis in cancer, Carcinogenesis 21 (2000) 485–495, https://doi.org/10.1093/carcin/21.3.485.
[85] J. Yue, J.M. López, Understanding MAPK signaling pathways in apoptosis, Int. J. Mol. Sci. 21 (2020) 2346, https://doi.org/10.3390/ijms21072346.
[86] M. Maaza, D. Hamidi, A. Simo, T. Kerdja, A.K. Chaudhary, J.K. Kana, Optical limiting in pulsed laser deposited VO_2 nanostructures, Opt. Commun. 6 (2012) 1190–1193, https://doi.org/10.1016/j.optcom.2011.09.057.